CHAPTER 5

DIELECTRIC STUDIES

5.1 Dielectric Relaxation Studies

In this chapter, further insight into the dynamic characteristics of ion motion will be obtained from the dielectric properties of the samples. The dielectric constant, ε_r and dielectric loss, ε_i were calculated from the impedance data obtained between 50 Hz and 1 MHz for the samples in the binary systems. The real and imaginary parts of the complex permittivity, $\varepsilon(\omega)$ and electrical modulus, M(ω) are given as follow:

$$\varepsilon_r(\omega) = \frac{tZ_i}{\omega\varepsilon_0 A(Z_i^2 + Z_r^2)}$$

$$\varepsilon_i(\omega) = \frac{tZ_r^2}{\omega\varepsilon_0 A(Z_i^2 + Z_r^2)}$$

And

$$\mathrm{M}_r(\omega) = \frac{\varepsilon_r}{(\varepsilon_r^2 + \varepsilon_i^2)}$$

$$\mathrm{M}_i(\omega) = \frac{\varepsilon_r}{(\varepsilon_r^2 + \varepsilon_i^2)}$$

Here ε_0 is the permittivity of free space, A is the electrode-pellet contact area, ω is the angular frequency and t is the thickness of the pellet.

Figure 5.1 show the frequency dependence of the dielectric constant for the samples with various AgI-CuI content at room temperature.

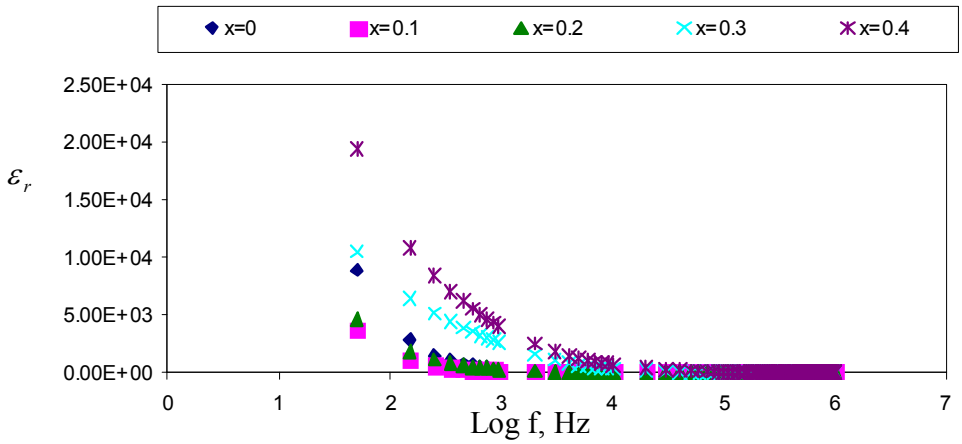

Figure 5.1: Real part of complex permittivity with frequency for AgI-CuI mixture.

It can be noticed that the trend of increase in ε_r at low frequencies is similar to the trend of conductivity versus CuI content.

Figure 5.2 show the frequency dependence of the dielectric loss for the samples with various AgI-CuI content at room temperature.

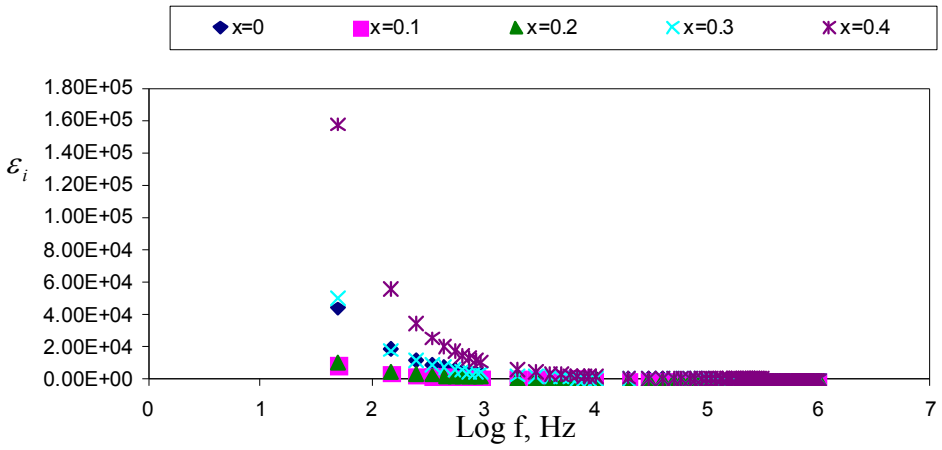

Figure 5.2: Imaginary part of complex permittivity with frequency for AgI-CuI mixture.

Variations of ε_r and ε_i with frequency at different temperatures are shown in the following sections.

5.2 Variation of ε_r with frequency at different temperatures for *x*CuI-(1-*x*)AgI, ($0 \leq x \leq 0.4$)

ε_r versus frequency for AgI at temperatures investigated are shown in Figure 5.3 (*a*) to 5.3 (*l*).

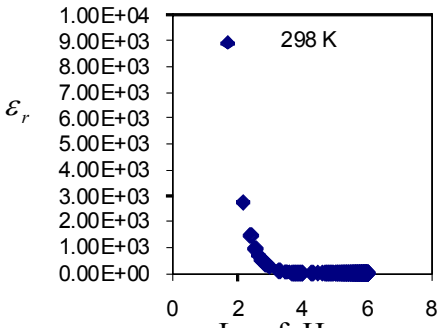

Figure 5.3 (*a*)

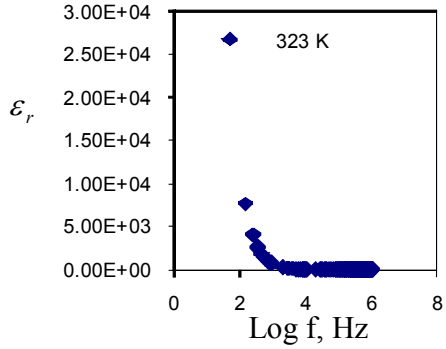

Figure 5.3 (*b*)

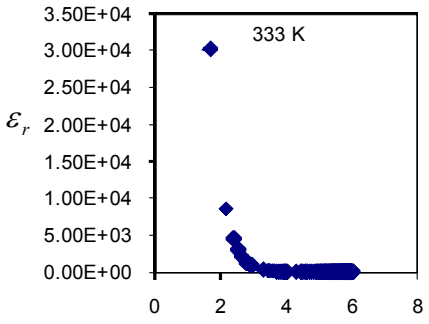

Figure 5.3 (*c*)

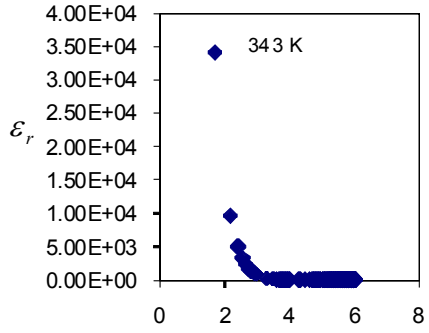

Figure 5.3 (*d*)

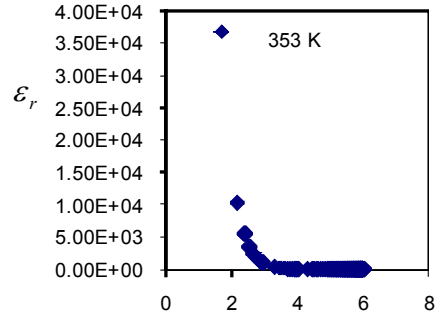

Figure 5.3 (*e*)

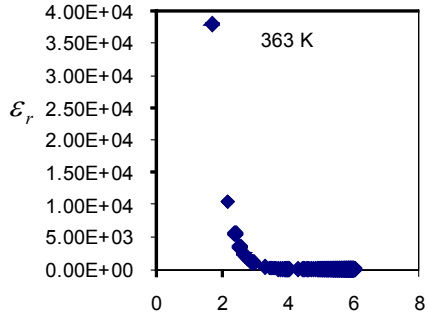

Figure 5.3 (*f*)

Continue …

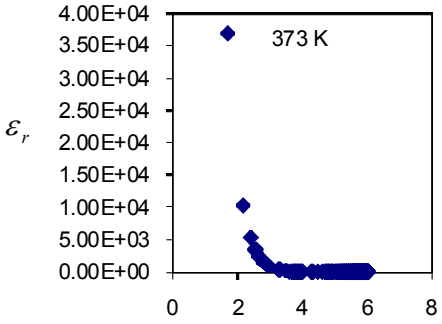

Figure 5.3 (*g*)

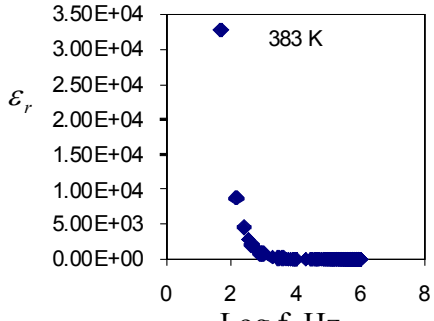

Figure 5.3 (*h*)

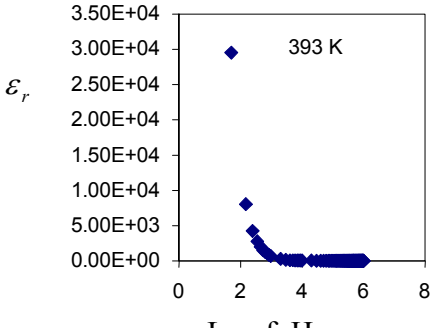

Figure 5.3 (*i*)

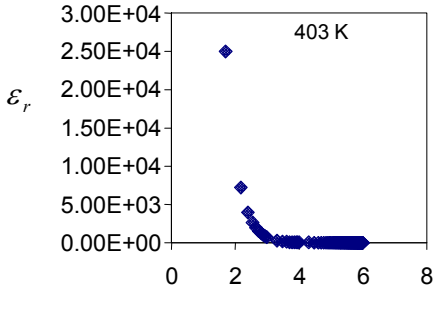

Figure 5.3 (*j*)

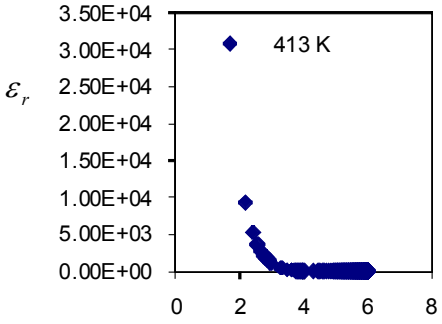

Figure 5.3 (*k*)

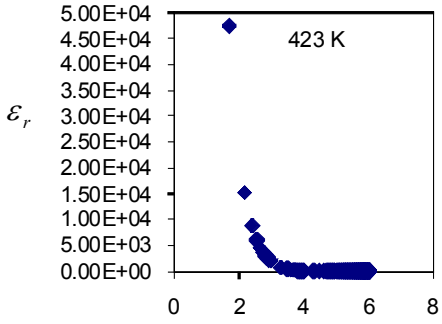

Figure 5.3 (*l*)

Figure 5.3: Plots of real part of complex permittivity with frequency at several temperatures for pure AgI.

It can be observed that at 50 Hz, the value of ε_r increases from 298 K to 363 K and then takes a dip from 373 K until 403 K and increases again at 413 K.

ε_r versus frequency for 0.1CuI-0.9AgI at temperatures investigated are shown in Figure 5.4 (*a*) to 5.4 (*l*).

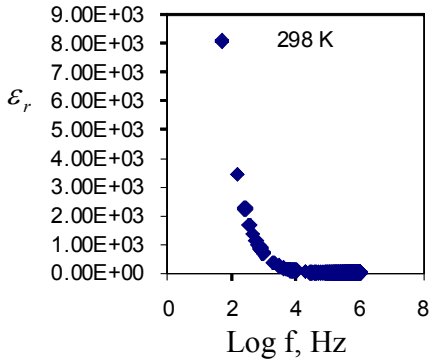

Figure 5.4 (*a*)

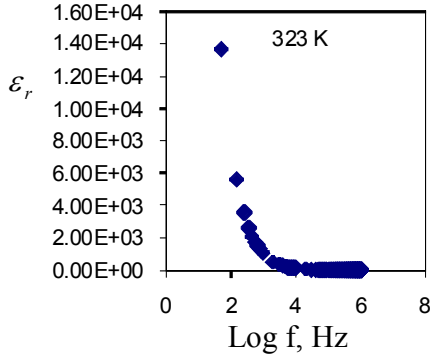

Figure 5.4 (*b*)

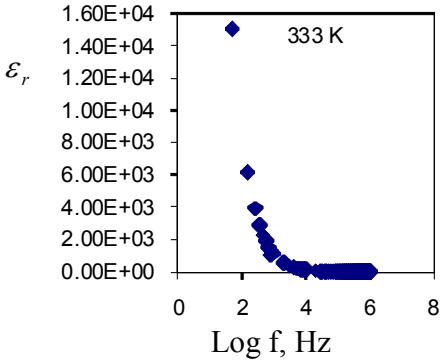

Figure 5.4 (*c*)

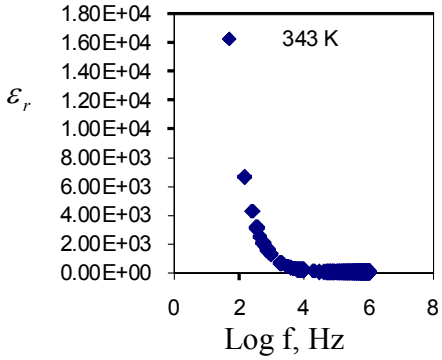

Figure 5.4 (*d*)

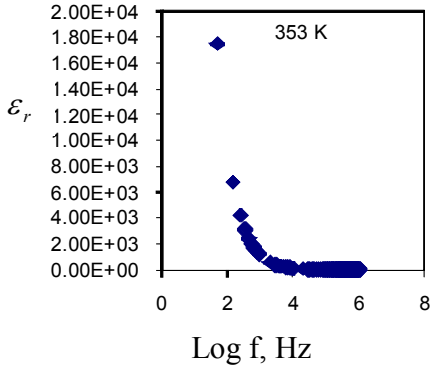

Figure 5.4 (*e*)

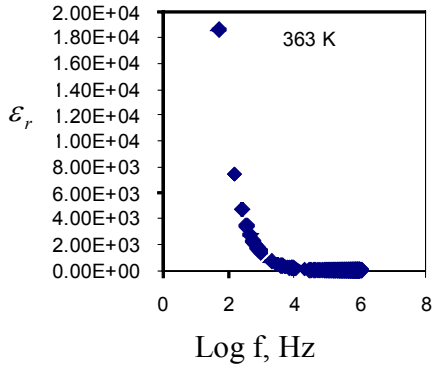

Figure 5.4 (*f*)

Continue …

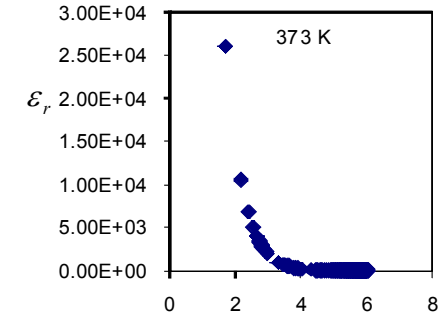

Figure 5.4 (*g*)

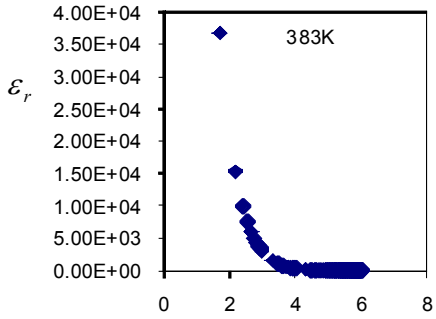

Figure 5.4 (*h*)

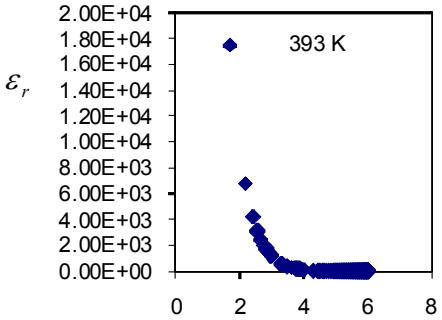

Figure 5.4 (*i*)

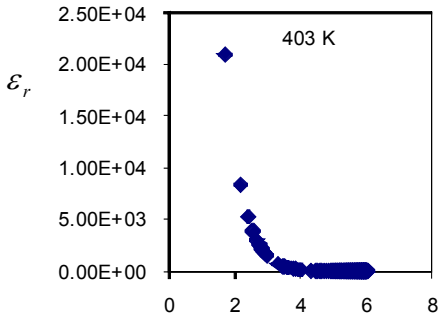

Figure 5.4 (*j*)

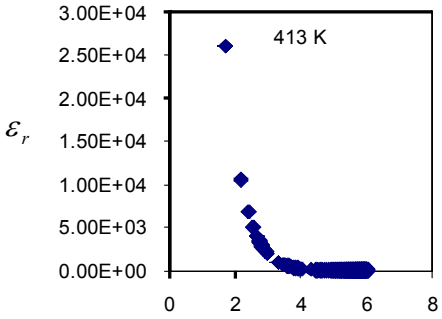

Figure 5.4 (*k*)

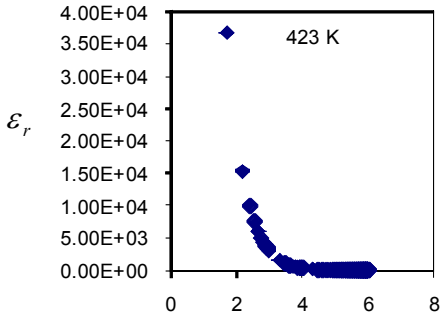

Figure 5.4 (*l*)

Figure 5.4: Plots of real part of complex permittivity with frequency at several temperatures for 0.1CuI-0.9AgI.

The same trend in variation of ε_r at 50 Hz is observed for 0.1CuI-0.9AgI as in pure AgI but at 393 K ε_r increases again.

ε_r versus frequency for 0.2CuI-0.8AgI at temperatures investigated are shown in Figure 5.5 (*a*) to 5.5 (*l*).

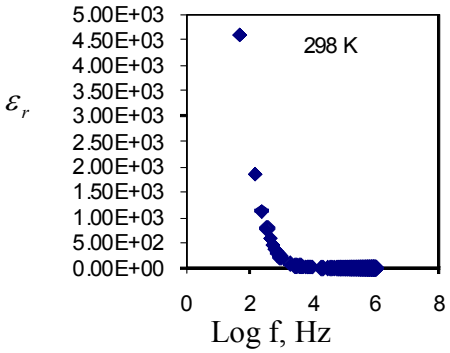

Figure 5.5 (*a*)

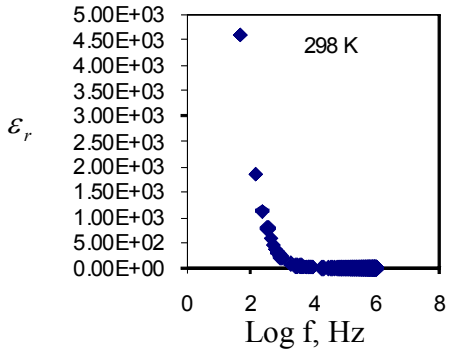

Figure 5.5 (*b*)

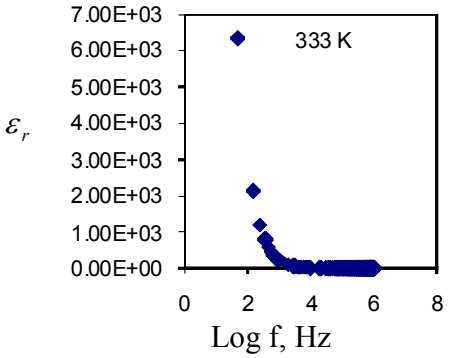

Figure 5.5 (*c*)

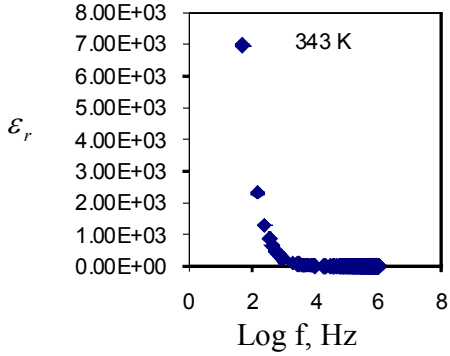

Figure 5.5 (*d*)

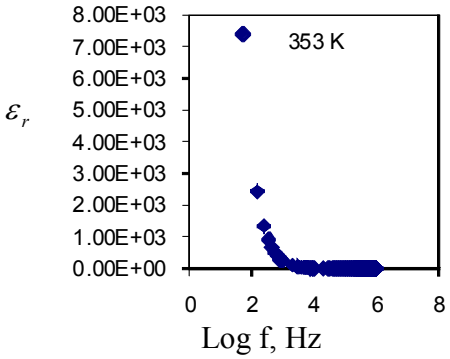

Figure 5.5 (*e*)

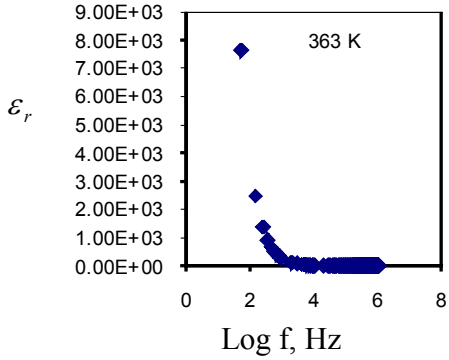

Figure 5.5 (*f*)

Continue …

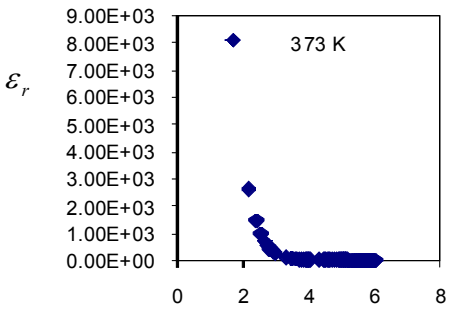

Figure 5.5 (*g*)

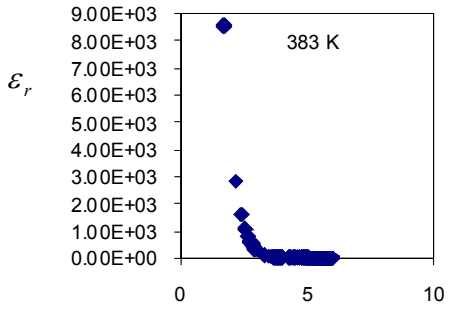

Figure 5.5(*h*)

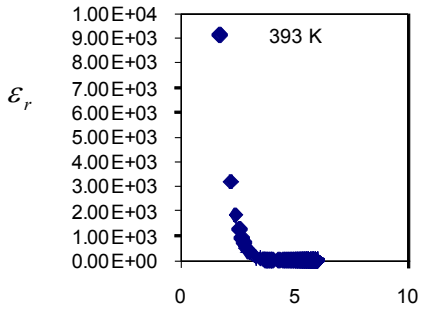

Figure 5.5 (*i*)

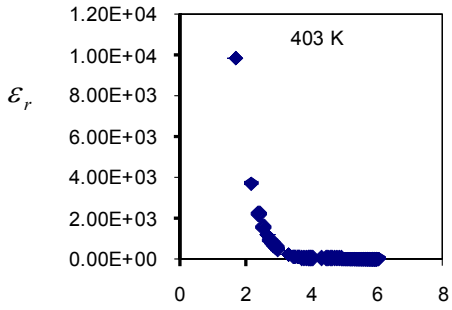

Figure 5.5 (*j*)

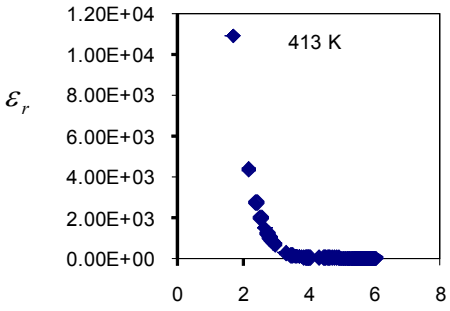

Figure 5.5 (*k*)

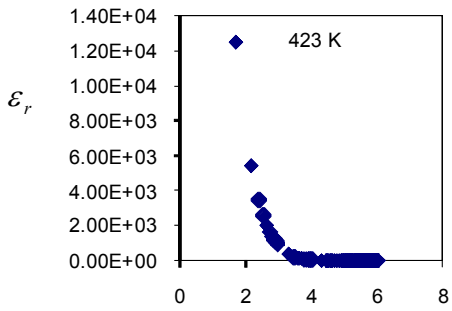

Figure 5.5 (*l*)

Figure 5.5: Plots of real part of complex permittivity with frequency at several temperatures for 0.2CuI-0.8AgI.

Unlike that of pure AgI and 0.1CuI-0.9AgI, ε_r increases with temperature as observed at 50 Hz. This indicates that more ions are accumulating at the electrode-sample interface implying that temperature assists in conductivity.

ε_r versus frequency for 0.3CuI-0.7AgI at temperatures investigated are shown in Figure 5.6 (*a*) to 5.6 (*l*).

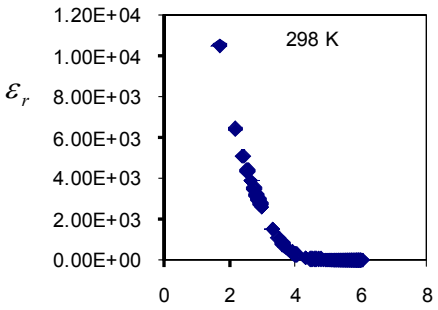

Figure 5.6 (*a*)

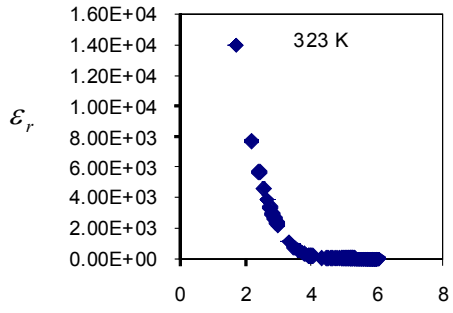

Figure 5.6 (*b*)

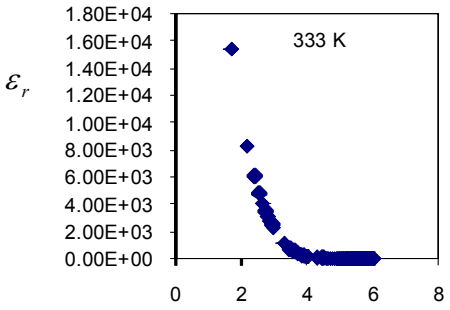

Figure 5.6 (*c*)

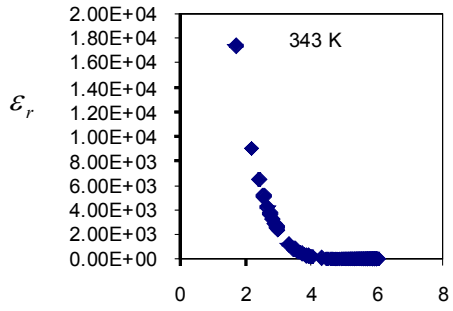

Figure 5.6 (*d*)

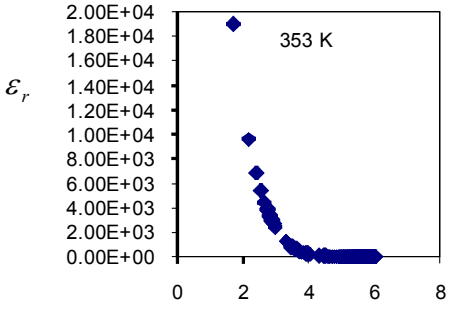

Figure 5.6 (*e*)

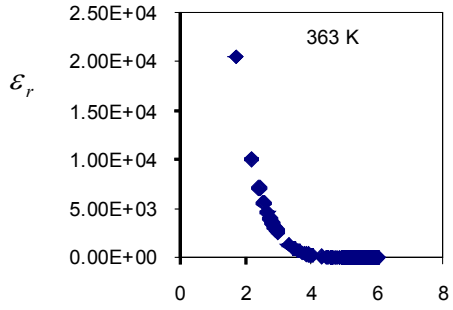

Figure 5.6 (*f*)

Continue …

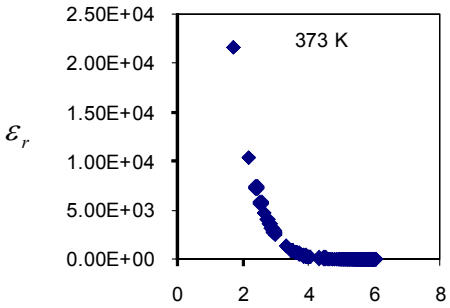

Figure 5.6 (*g*)

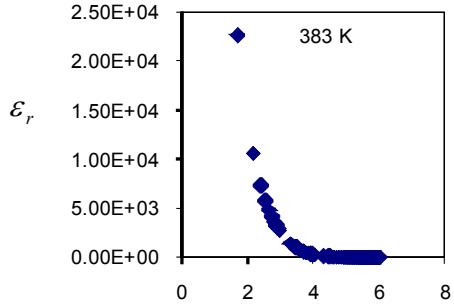

Figure 5.6 (*h*)

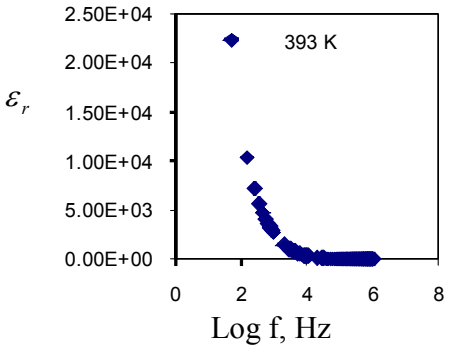

Figure 5.6 (*i*)

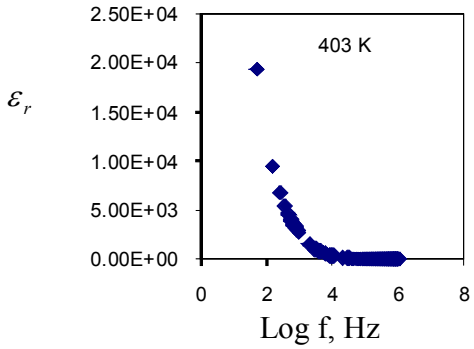

Figure 5.6 (*j*)

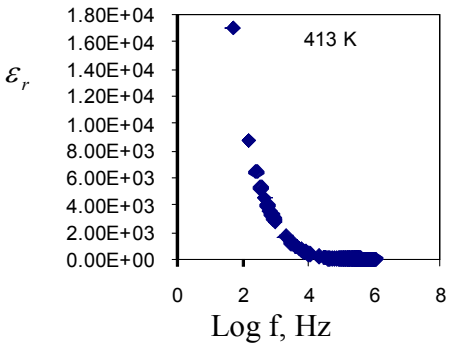

Figure 5.6 (*k*)

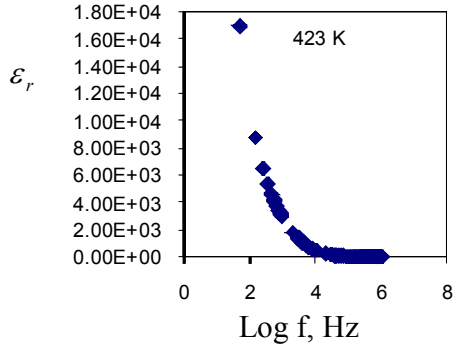

Figure 5.6 (*l*)

Figure 5.6: Plots of real part of complex permittivity with frequency at several temperatures for 0.3CuI-0.7AgI.

A drop in ε_r value is observed beginning from 403 K at 50 Hz.

ε_r versus frequency for 0.4CuI-0.6AgI at temperatures investigated are shown in Figure 5.7 (*a*) to 5.7 (*l*).

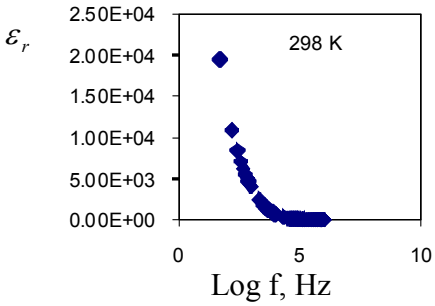

Figure 5.7 (*a*)

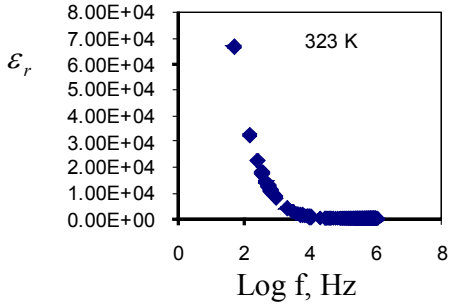

Figure 5.7 (*b*)

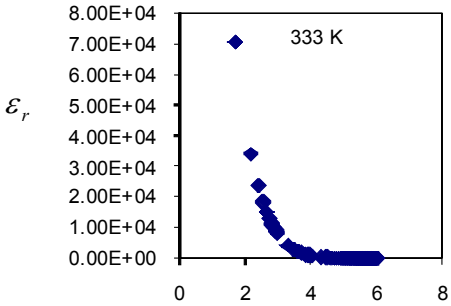

Figure 5.7 (*c*)

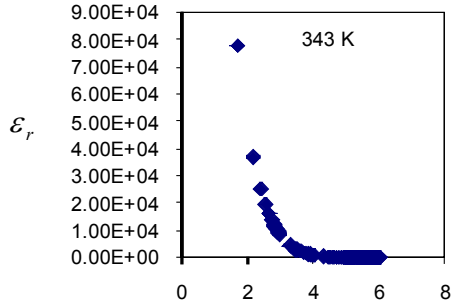

Figure 5.7 (*d*)

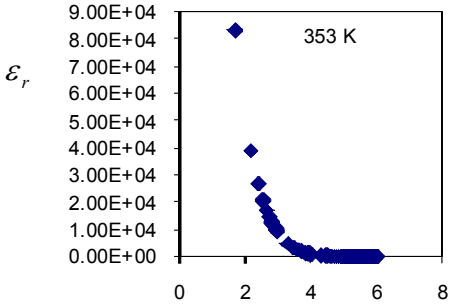

Figure 5.7 (*e*)

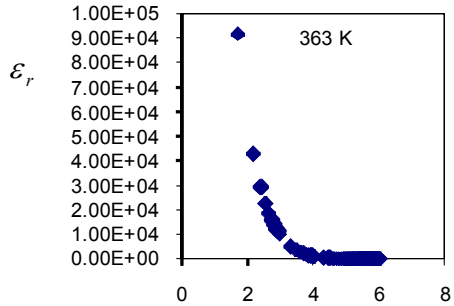

Figure 5.7 (*f*)

Continue …

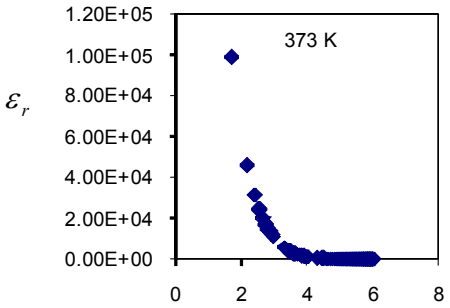

Figure 5.7 (*g*)

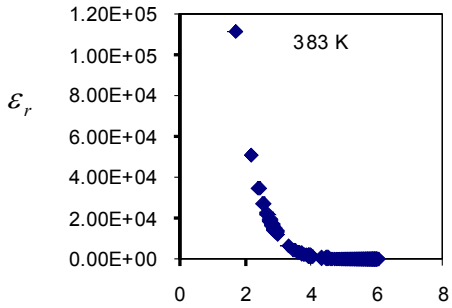

Figure 5.7 (*h*)

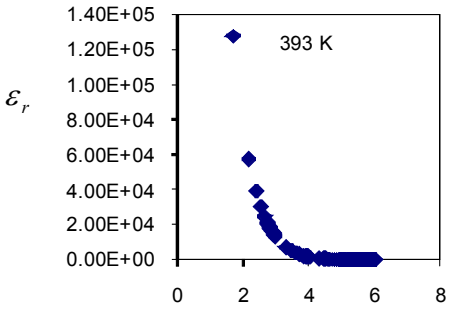

Figure 5.7 (*i*)

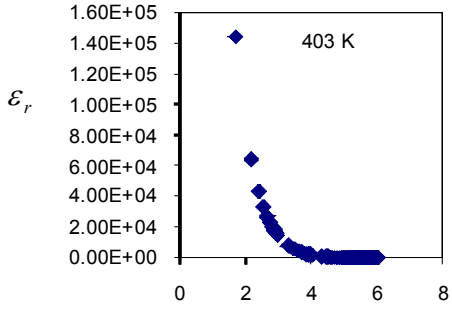

Figure 5.7 (*j*)

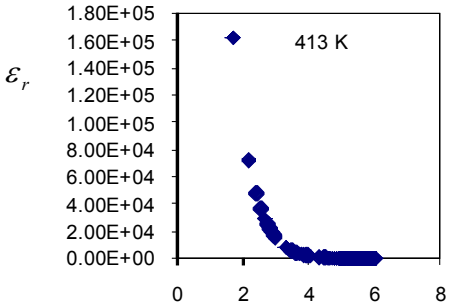

Figure 5.7 (*k*)

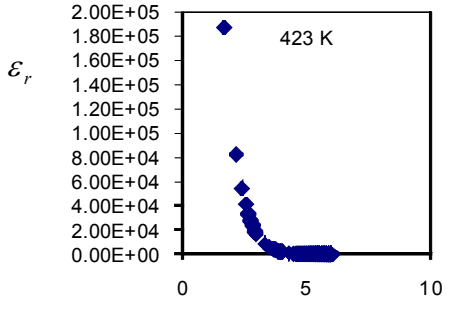

Figure 5.7 (*l*)

Figure 5.7: Plots of real part of complex permittivity with frequency at several temperatures for 0.4CuI-0.6AgI.

No significant decrease in ε_r is observed for 0.4CuI-0.6AgI in the temperature range from 298 K to 423 K.

5.3 Variation of ε_i with frequency at different temperatures for *x*CuI-(1-*x*)AgI, ($0 \leq x \leq 0.4$)

ε_i versus frequency for AgI at temperatures investigated are shown in Figure 5.8 (*a*) to 5.8 (*l*).

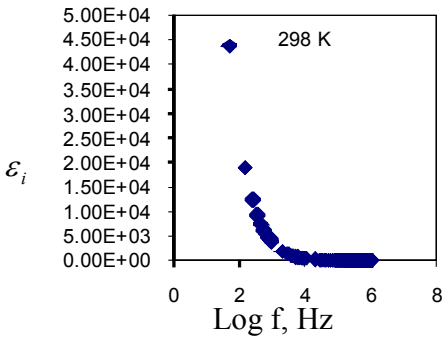

Figure 5.8 (*a*)

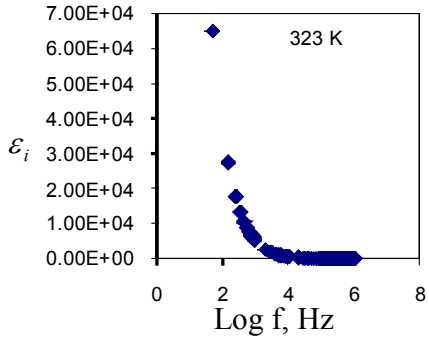

Figure 5.8 (*b*)

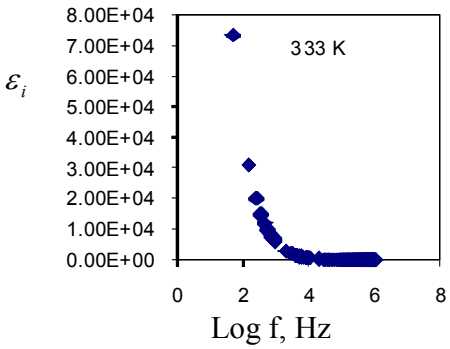

Figure 5.8 (*c*)

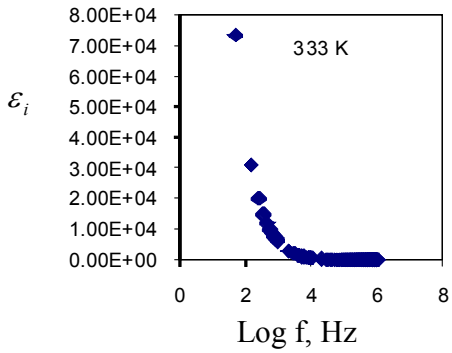

Figure 5.8 (*d*)

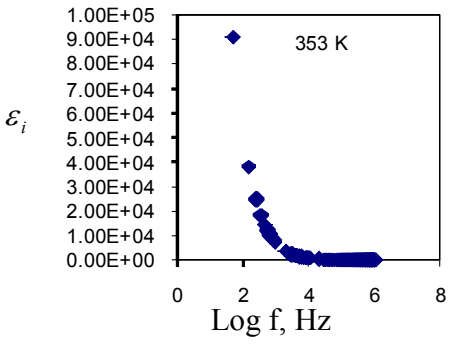

Figure 5.8 (*e*)

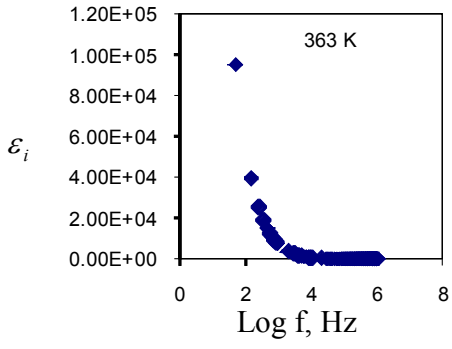

Figure 5.8 (*f*)

Continue …

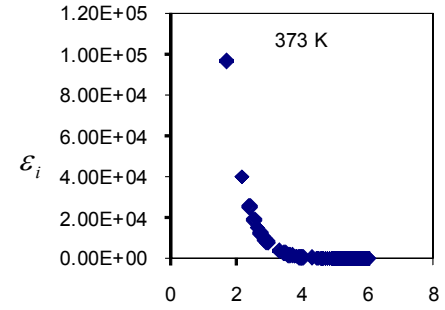

Figure 5.8 (*h*)

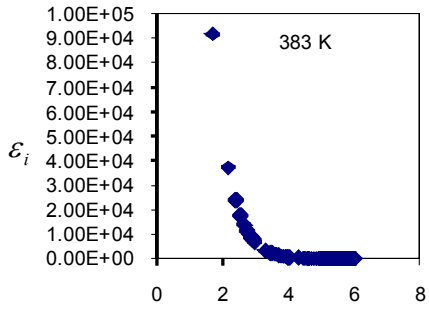

Figure 5.8 (*i*)

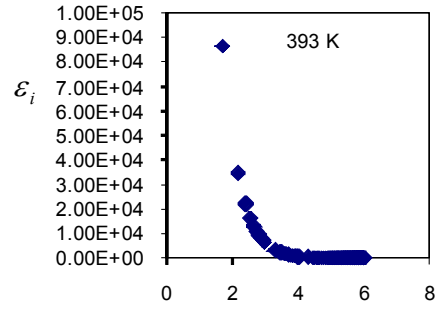

Figure 5.8 (*i*)

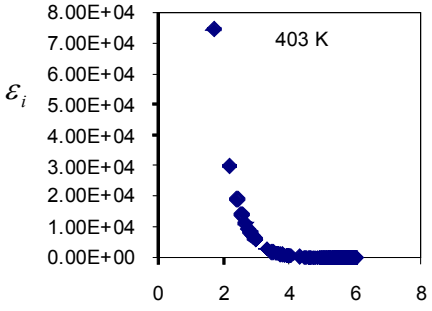

Figure 5.8 (*j*)

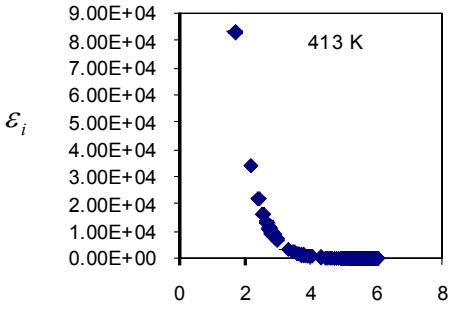

Figure 5.8 (*k*)

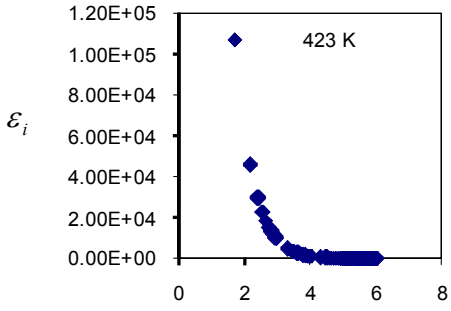

Figure 5.8 (*l*)

Figure 5.8: Plots of imaginary part of complex permittivity with frequency at several temperatures for pure AgI

Variation in ε_i with temperature at 50 Hz is similar to ε_r for pure AgI.

ε_i versus frequency for 0.1CuI-0.9AgI at temperatures investigated are shown in Figure 5.9 (*a*) to 5.9 (*l*).

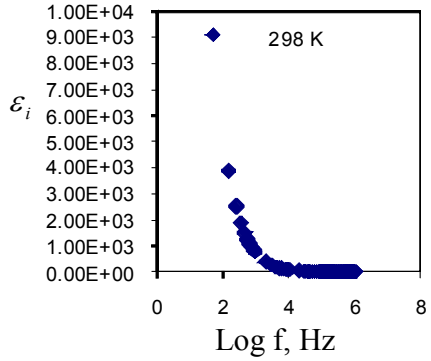

Figure 5.9 (*a*)

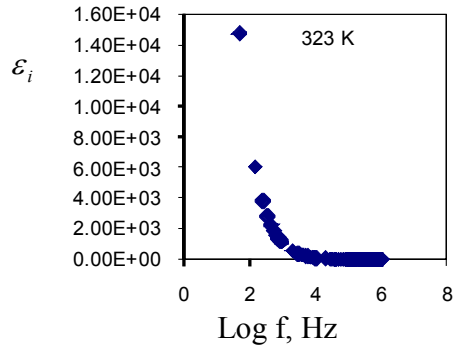

Figure 5.9 (*b*)

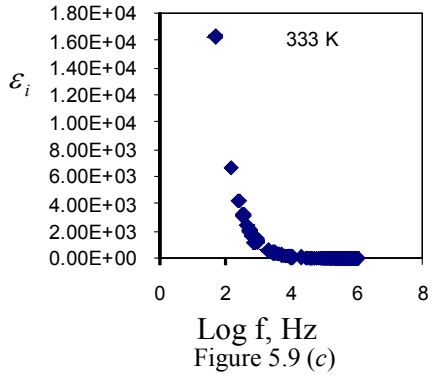

Figure 5.9 (*c*)

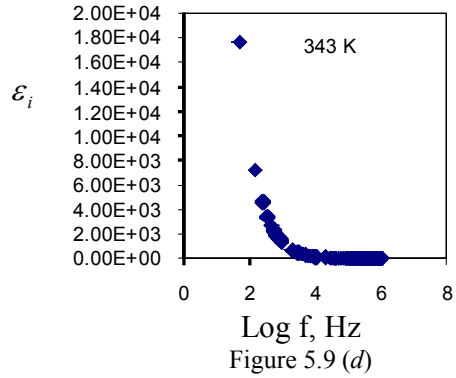

Figure 5.9 (*d*)

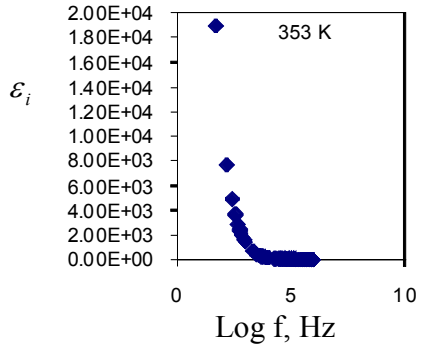

Figure 5.9 (*e*)

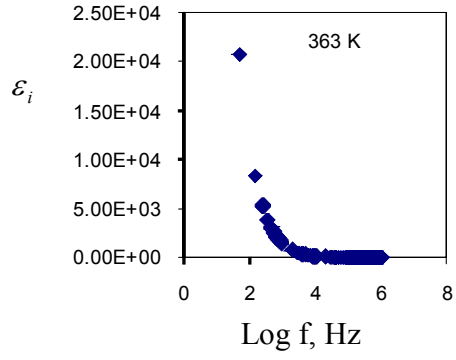

Figure 5.9 (*f*)

Continue …

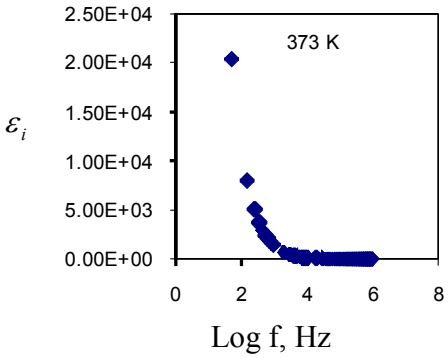

Figure 5.9 (*g*)

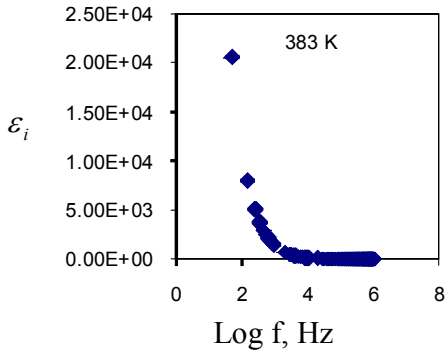

Figure 5.9 (*h*)

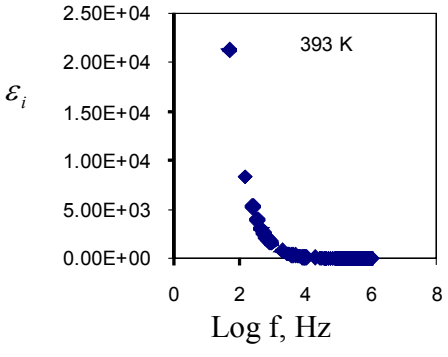

Figure 5.9 (*i*)

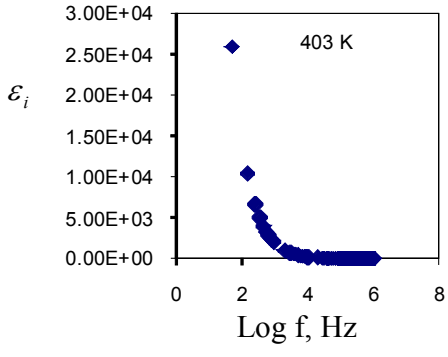

Figure 5.9 (*j*)

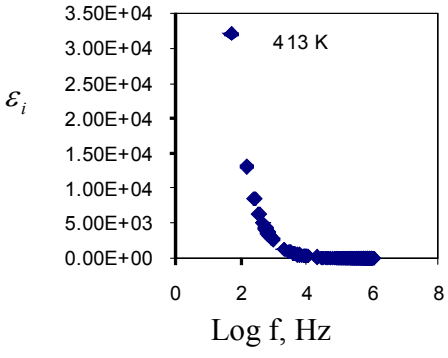

Figure 5.9 (*k*)

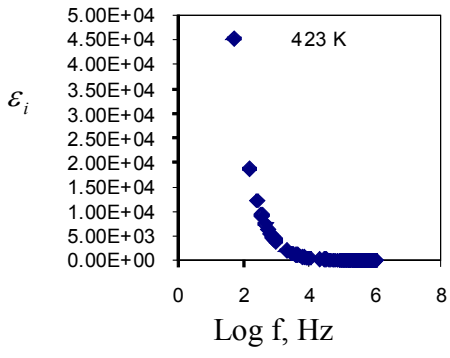

Figure 5.9 (*l*)

Figure 5.9: Plots of imaginary part of complex permittivity with frequency at several temperatures for 0.1CuI-0.9AgI.

Temperature is observed to affect the value of ε_i at 50 Hz in the same manner as for ε_r

ε_i versus frequency for 0.2CuI-0.8AgI at temperatures investigated are shown in Figure 5.10 (*a*) to 5.10 (*l*).

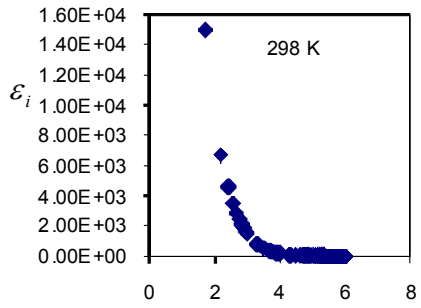

Figure 5.10 (*a*)

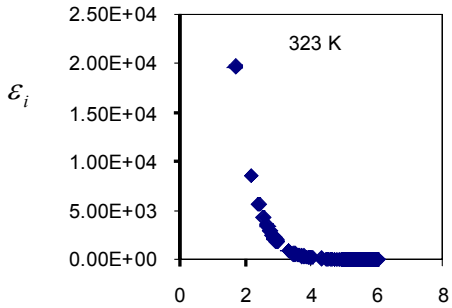

Figure 5.10 (*b*)

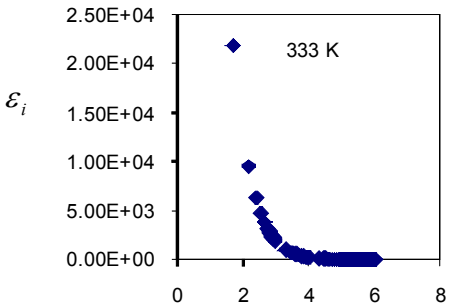

Figure 5.10 (*c*)

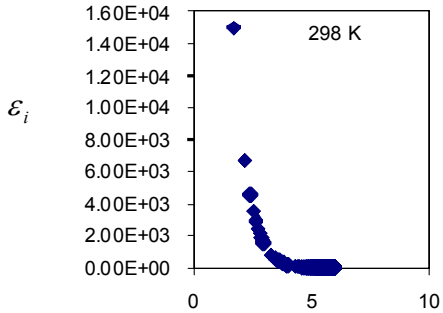

Figure 5.10 (*d*)

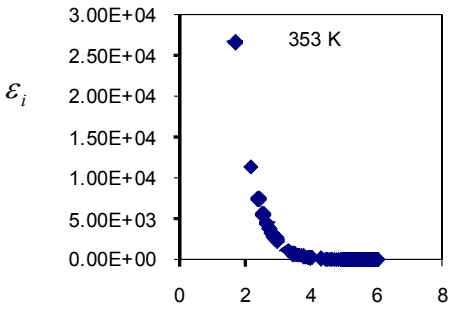

Figure 5.10 (*e*)

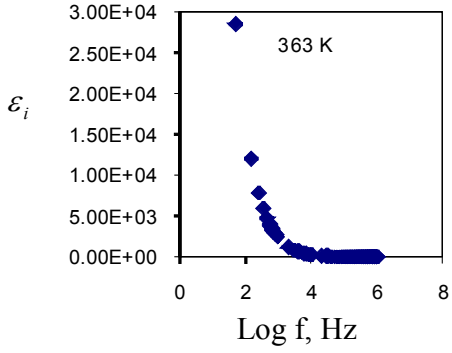

Figure 5.10 (*f*)

Continue …

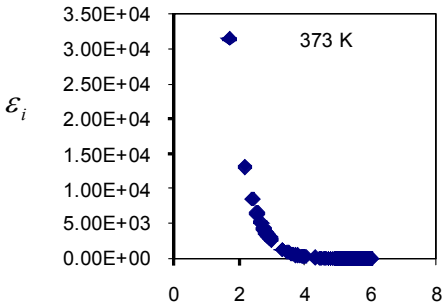

Figure 5.10 (*g*)

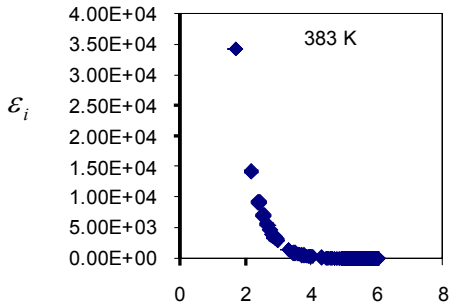

Figure 5.10 (*h*)

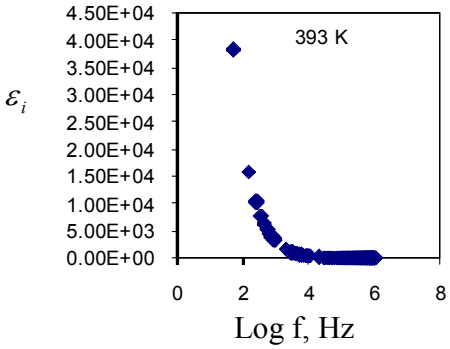

Figure 5.10 (*i*)

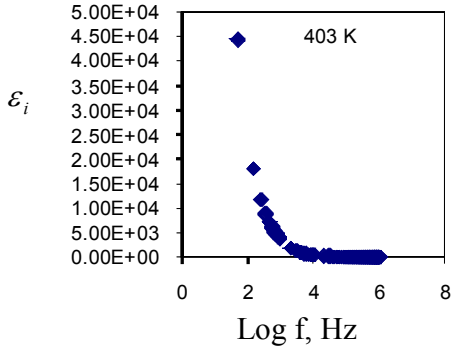

Figure 5.10 (*j*)

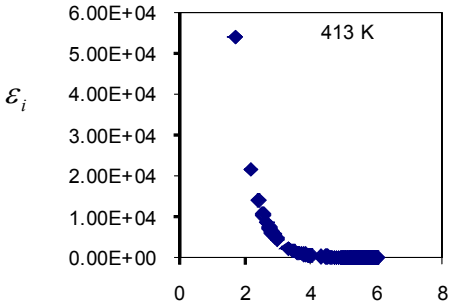

Figure 5.10 (*k*)

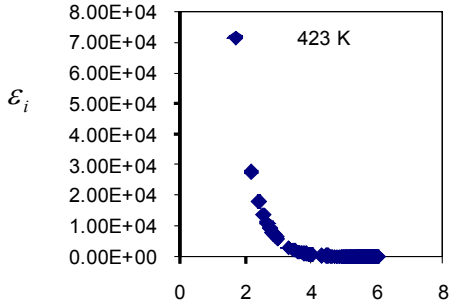

Figure 5.10 (*l*)

Figure 5.10: Plots of imaginary part of complex permittivity with frequency at several temperatures for 0.2CuI-0.8AgI.

ε_i increases for all temperatures at 50 Hz. Similar with ε_r

ε_i versus frequency for 0.3CuI-0.7AgI at temperatures investigated are shown in Figure 5.11 (*a*) to 5.11 (*l*).

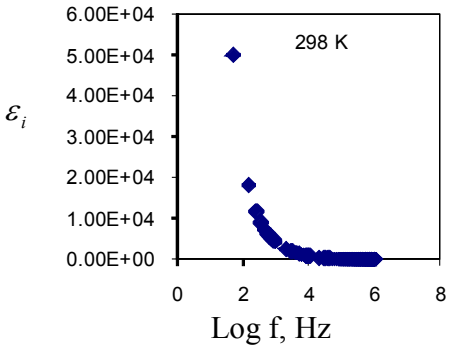

Figure 5.11 (*a*)

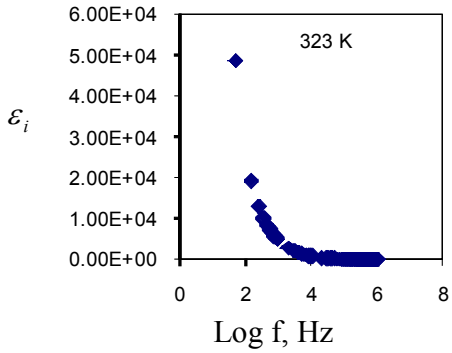

Figure 5.11 (*b*)

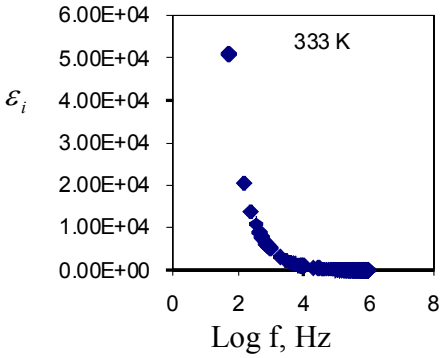

Figure 5.11 (*c*)

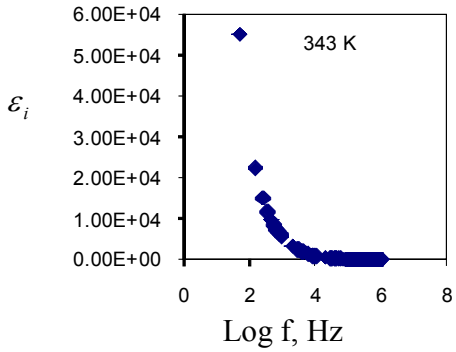

Figure 5.11 (*d*)

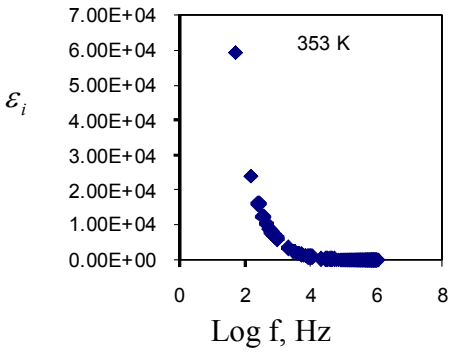

Figure 5.11 (*e*)

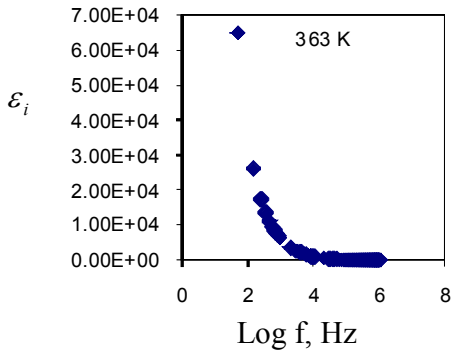

Figure 5.11 (*f*)

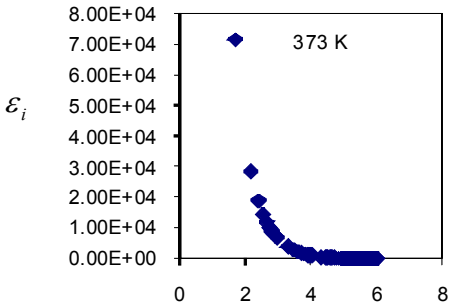

Figure 5.11 (*g*)

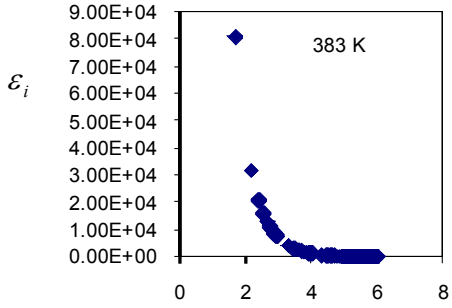

Figure 5.11 (*h*)

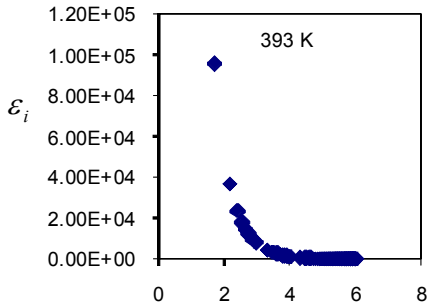

Figure 5.11 (*i*)

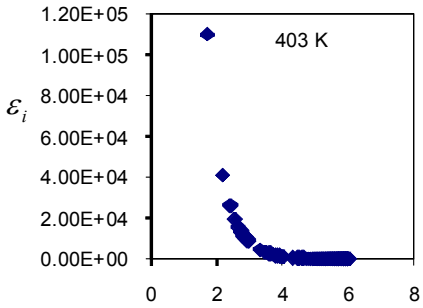

Figure 5.11 (*j*)

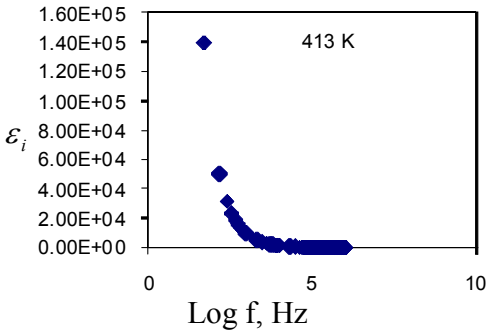

Figure 5.11 (*k*)

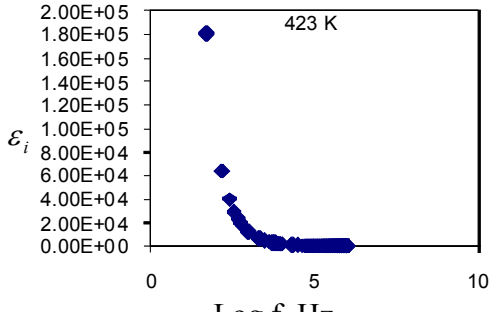

Figure 5.11 (*l*)

Figure 5.11: Plots of imaginary part of complex permittivity with frequency at several temperatures for 0.3CuI-0.7AgI.

A dip is observed at 323 K for ε_i at 50 Hz.

ε_i versus frequency for 0.4CuI-0.6AgI at temperatures investigated are shown in Figure 5.12 (*a*) to 5.12 (*l*).

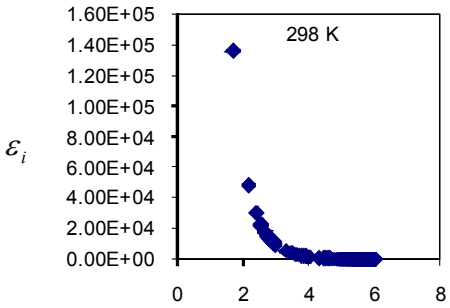

Figure 5.12 (*a*)

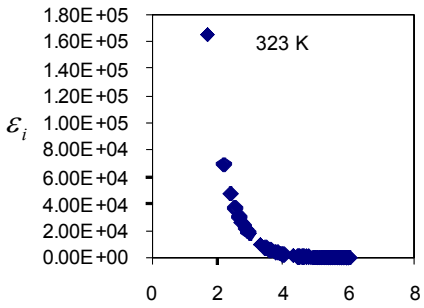

Figure 5.12 (*b*)

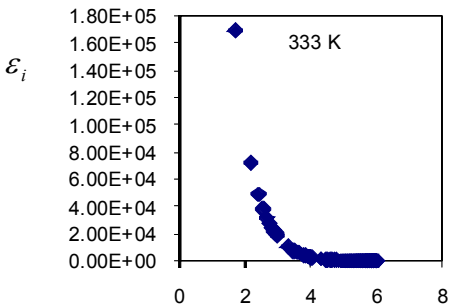

Figure 5.12 (*c*)

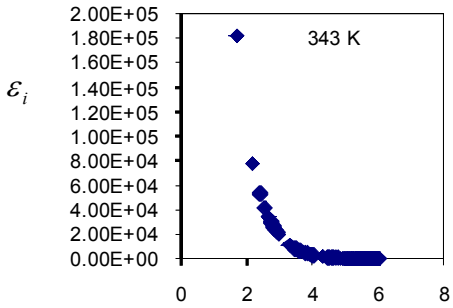

Figure 5.12 (*d*)

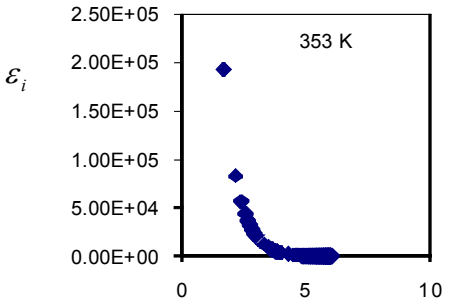

Figure 5.12 (*e*)

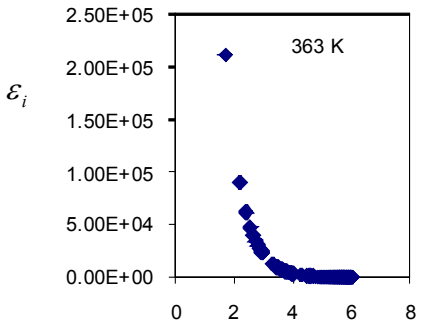

Figure 5.12 (*f*)

Continue …

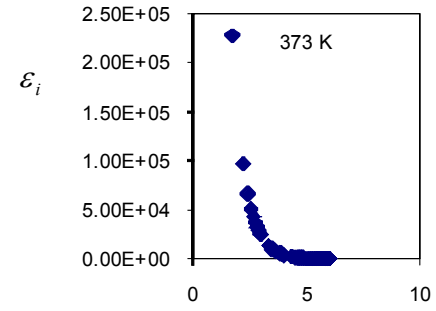

Figure 5.12 (*g*)

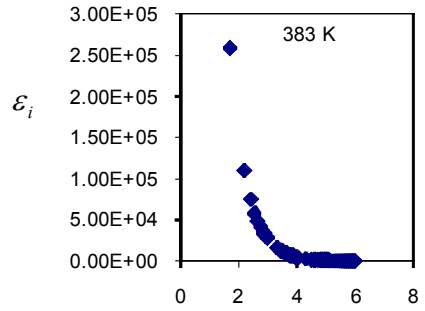

Figure 5.12 (*h*)

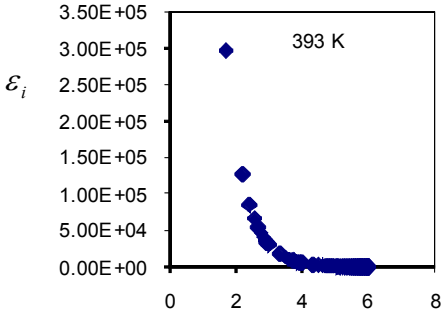

Figure 5.12 (*i*)

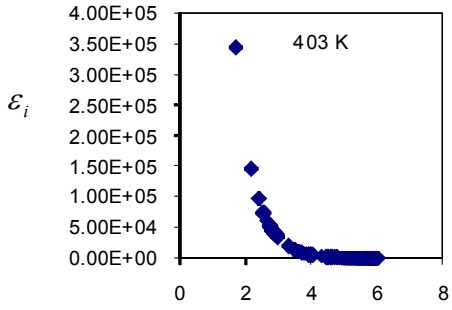

Figure 5.12 (*j*)

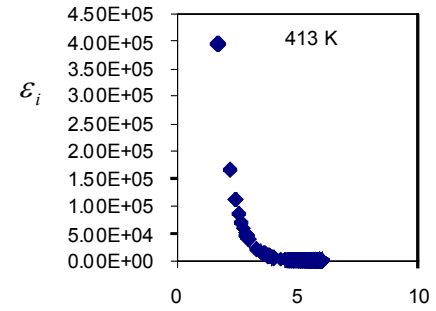

Figure 5.12 (*k*)

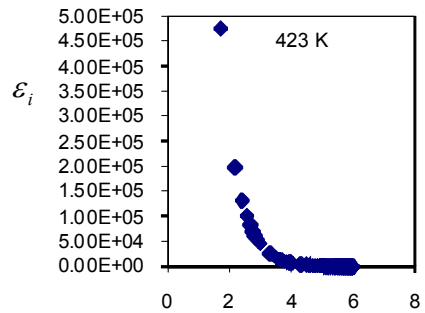

Figure 5.12 (*l*)

Figure 5.12: Plots of imaginary part of complex permittivity with frequency at several temperatures for 0.4CuI-0.6AgI.

ε_i increases for all temperatures at 50 Hz as for ε_r

It can be seen that the dielectric constant and dielectric loss decreases with increasing in frequency and saturates at high frequencies. In the low frequency region, the behavior of the dielectric constant and dielectric loss can be associated with space charge effect arising from the electrodes (Almond et.al, 1984). The effect of electrode polarization also causes the decrement of a.c conductivity at the lower frequencies. Since there is no appreciable relaxation peaks observed, the dielectric constant, ε_r and dielectric loss, ε_i in this study was used as an indicator to show that the increase in conductivity is mainly due to the increment in number density of the charge carriers. The observed variations in ε_r and ε_i versus frequency for the samples could be attributed to the build-up of space charge region in the electrode-pellet interface as the different relaxation times of the ions.

At low frequency region, the dielectric constant, ε_r and dielectric loss, ε_i is proportional to ω^{n-1} indicating non-Debye dependence implying that the conductivity exhibits relaxation that is non-exponential in time. This dispersion reflects the existence of space charge polarization where there is time for the charges to build up at the interface before the applied field changes direction and hence, the large values of ε_r and ε_i are obtained.

On the other hand, with the increase in frequency, there is no time for the charges to build up at the interface because of the increasing reversal rate of the electric field. Therefore, the polarization due to charge accumulation decreases which leads to the decrease in the values of ε_r and ε_i.

5.4 Transport mechanism of ions

The ac conductivity of *x*CuI-(1-*x*)AgI can be obtained from dielectric constant, ε_r and loss tangent, tan δ at every frequency according to

$$\sigma_{ac} = \varepsilon_0 \varepsilon_r \omega \tan\delta \tag{5.1}$$

Since $\tan\delta = \frac{\varepsilon_i}{\varepsilon_r}$,

$$\therefore \sigma_{ac} = \varepsilon_0 \varepsilon_i \omega \tag{5.2}$$

Here ε_i is the dielectric loss, angular frequency, $\omega = 2\pi f$, f is the frequency and ε_0 is the vacuum permittivity (8.854 x 10^{-14} F cm^{-1}).

From Jonscher's Universal Power Law:

$$\sigma_{ac} = A\omega^s \tag{5.3}$$

By equating equation (5.2) and equation (5.3),

$$\varepsilon_0 \varepsilon_i \omega = A\omega^s \tag{5.4}$$

$$\varepsilon_0 \varepsilon_i A = \omega^{s-1} \tag{5.5}$$

$$\ln \varepsilon_i = \ln \frac{A}{\varepsilon_0} + (s-1) \ln \omega \tag{5.6}$$

and

$$\varepsilon_i = \frac{Z_r}{\omega C_0 (Z_r^2 + Z_i^2)}$$

From equation 5.6, graphs of $\ln \varepsilon_i$ versus ln ω were plotted and the gradient, *m* of the graphs were determined. Since the ion hopping frequency, ω_p corresponds to twice σ_{dc}, hence, $\ln \varepsilon_i$ and $\ln \omega$ values were taken from $\ln \omega_p$ onwards. Values of s can be obtained from (*m*+1) where *m* is gradient of $ln\, \varepsilon_i$ versus $ln\, \omega$.

For the AgI sample, the graphs are depicted in Figure 5.13 (*a*) to 5.13 (*l*)

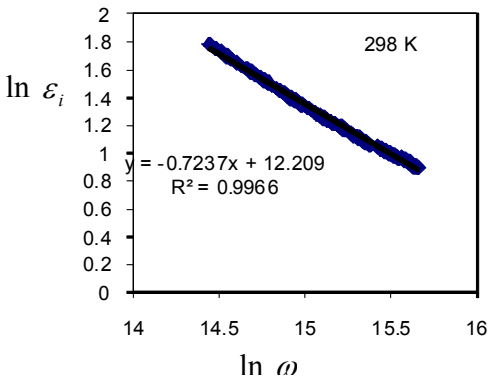

Figure 5.13 (*a*)

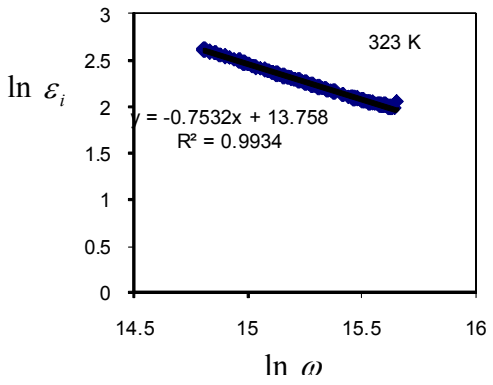

Figure 5.13 (*b*)

Continue …

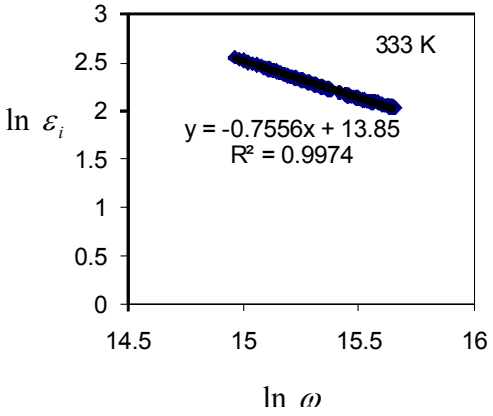

Figure 5.13 (*c*)

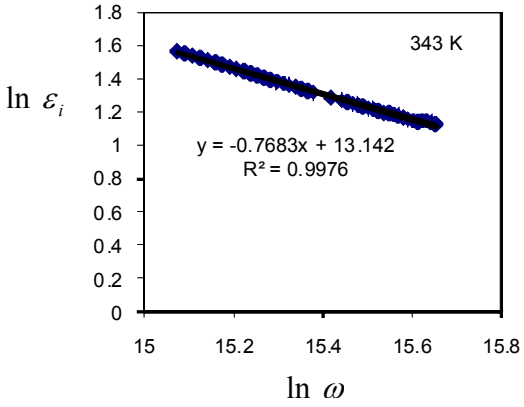

Figure 5.13 (*d*)

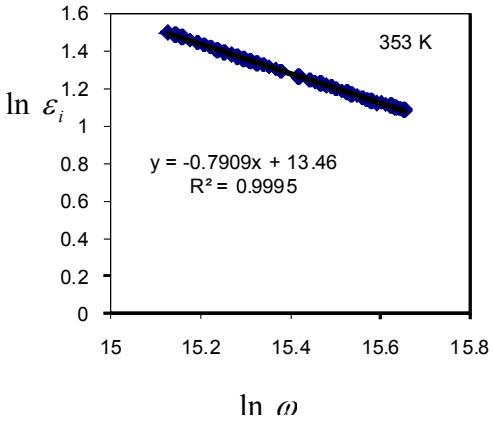

Figure 5.13 (*e*)

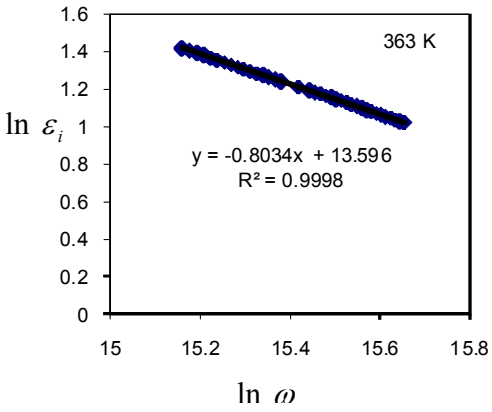

Figure 5.13 (*f*)

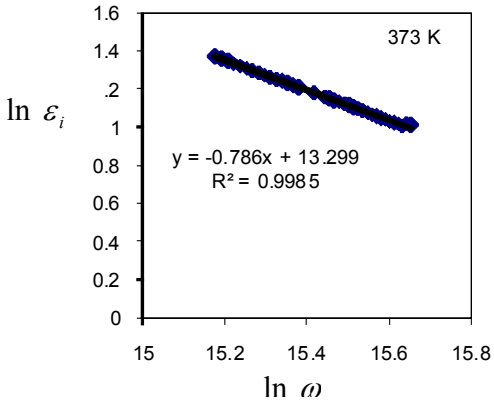

Figure 5.13 (*g*)

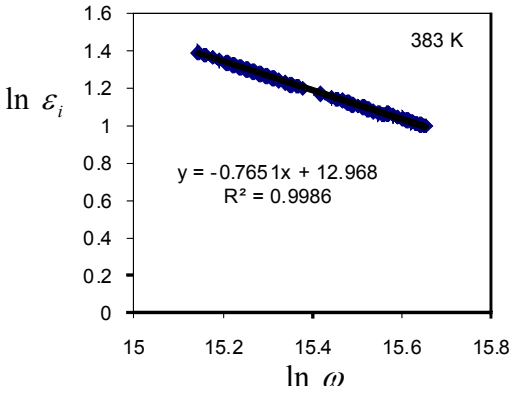

Figure 5.13 (*h*)

Continue …

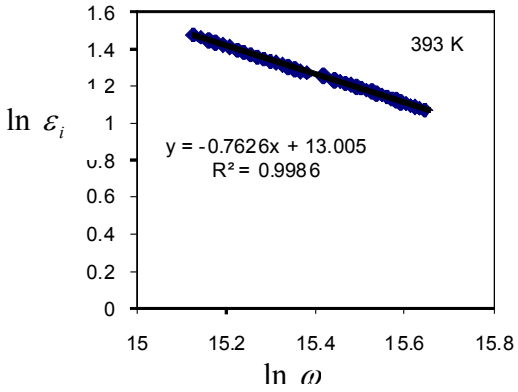

Figure 5.13 (*i*)

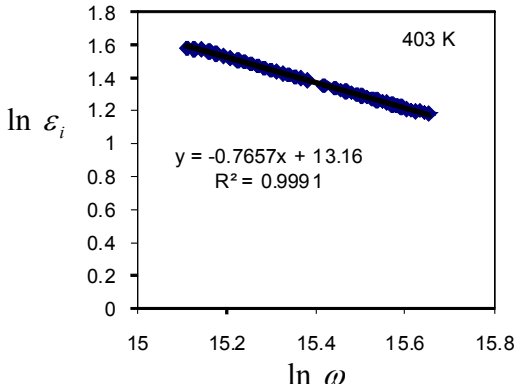

Figure 5.13 (*j*)

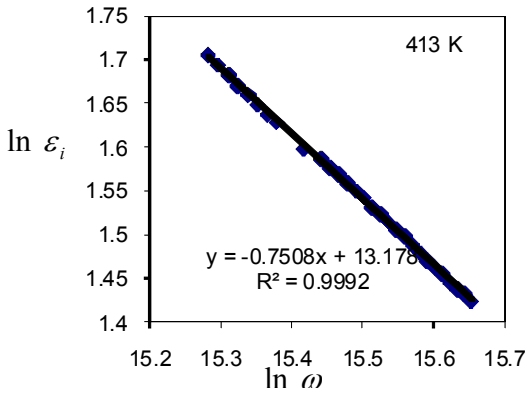

Figure 5.13 (*k*)

Figure 5.13: $\ln \varepsilon_i$ versus $\ln \omega$ (Hz) at various temperatures for pure AgI.

For the 0.1CuI-0.9AgI sample, the graphs are depicted in Figure 5.14(*a*) to 5.14(*l*)

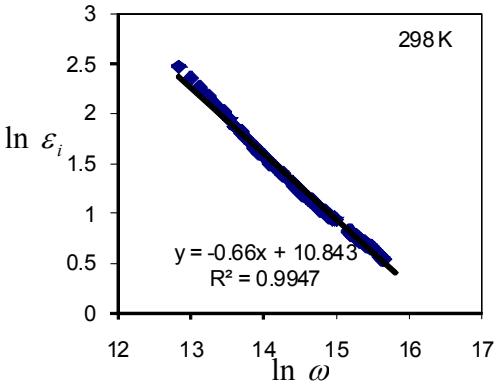

Figure 5.14 (*a*)

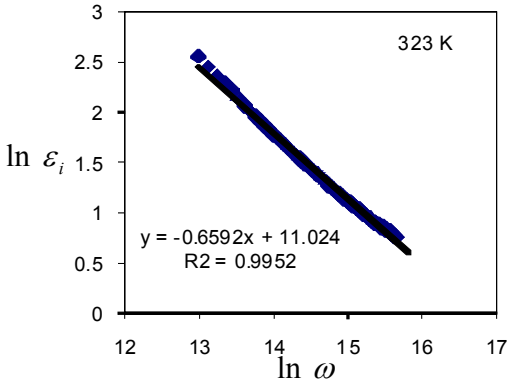

Figure 5.14 (*b*)

Continue …

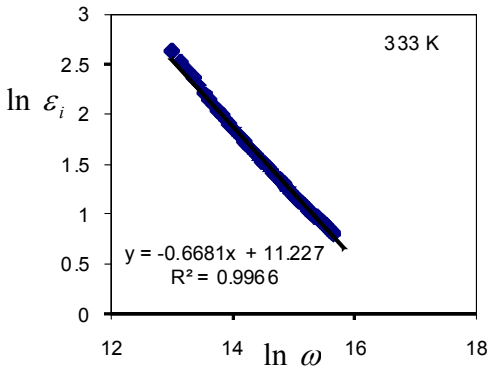

Figure 5.14 (*c*)

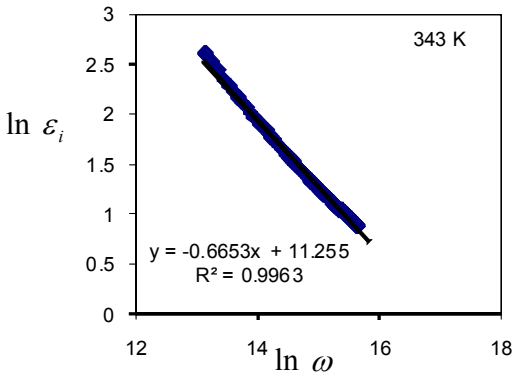

Figure 5.14 (*d*)

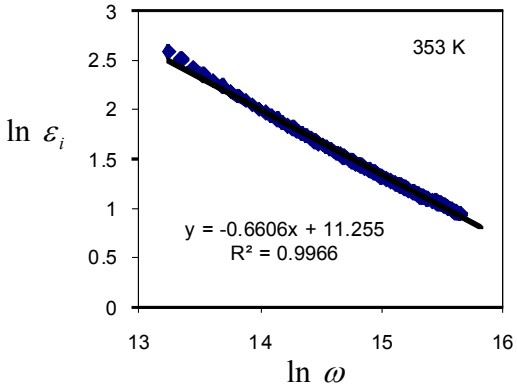

Figure 5.14 (*e*)

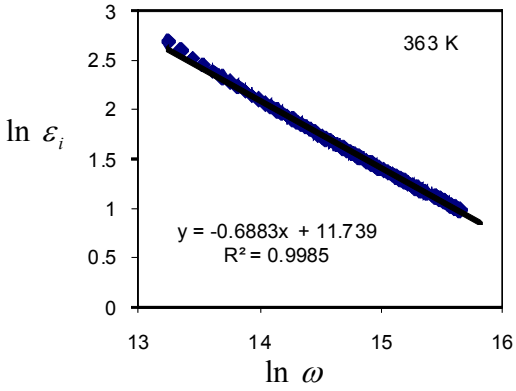

Figure 5.14 (*f*)

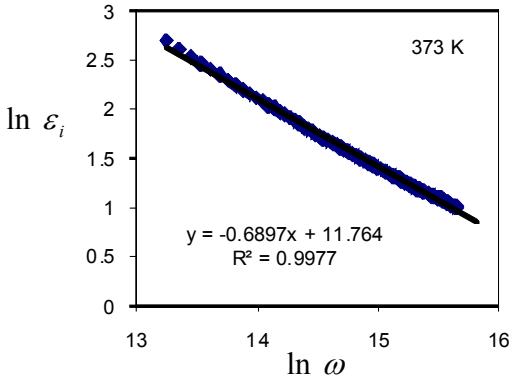

Figure 5.14 (*g*)

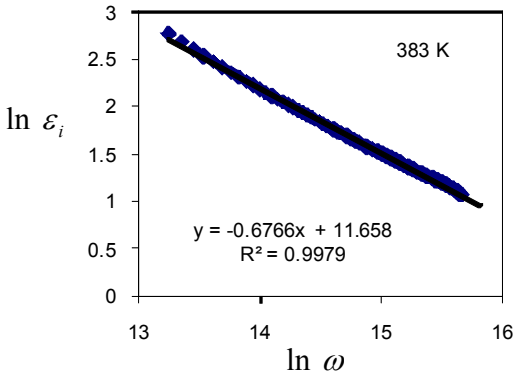

Figure 5.14 (*h*)

Continue …

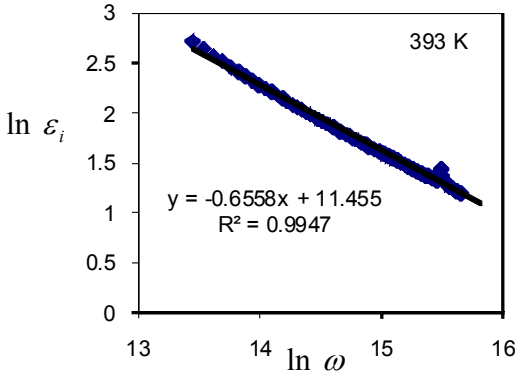

Figure 5.14 (*i*)

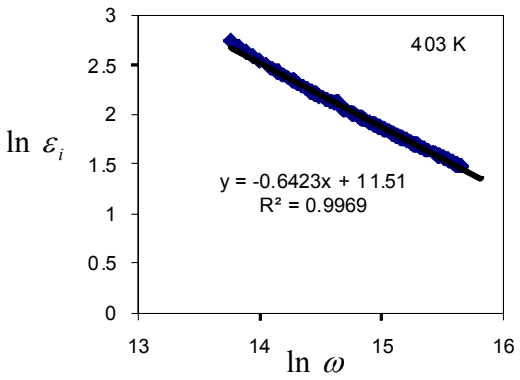

Figure 5.14 (*j*)

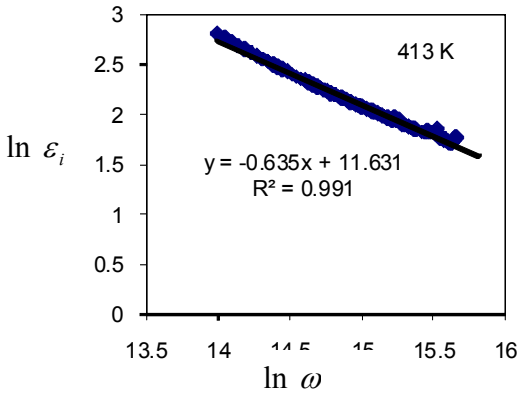

Figure 5.14 (*k*)

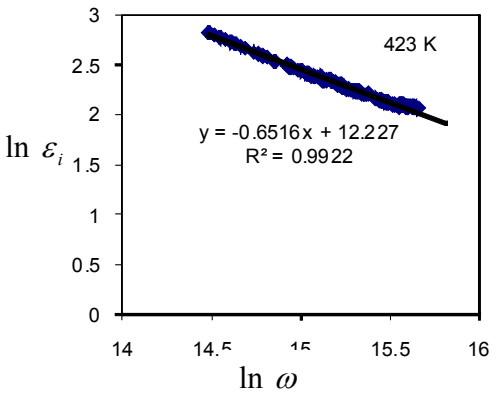

Figure 5.14 (*l*)

Figure 5.14: $\ln \varepsilon_i$ versus $\ln \omega$ (Hz) at various temperatures for 0.1CuI-0.9AgI.

For the 0.2CuI-0.8AgI sample, the graphs are depicted in Figure 5.15 (*a*) to 5.15 (*l*).

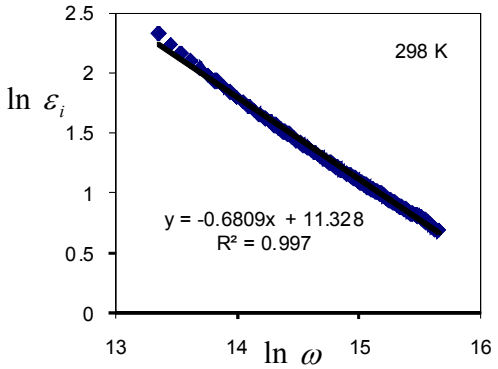

Figure 5.15 (*a*)

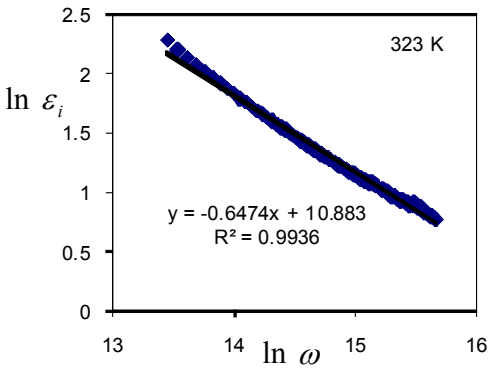

Figure 5.15 (*b*)

Continue …

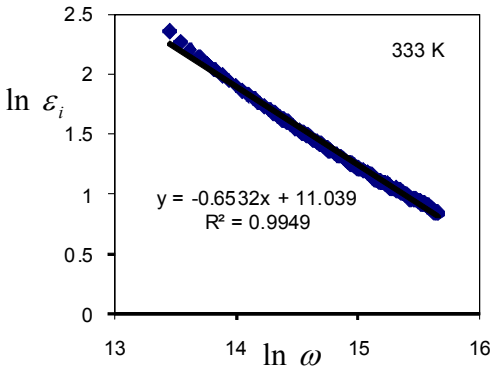

Figure 5.15 (*c*)

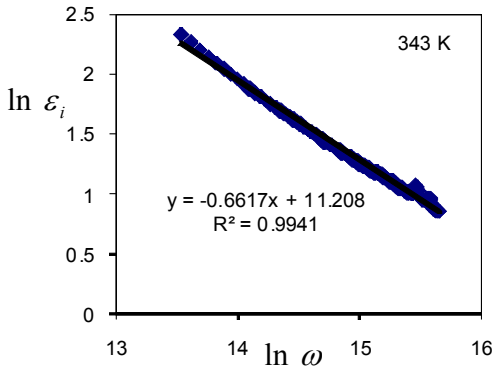

Figure 5.15 (*d*)

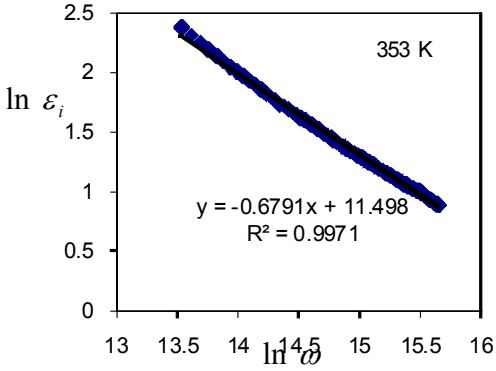

Figure 5.15 (*e*)

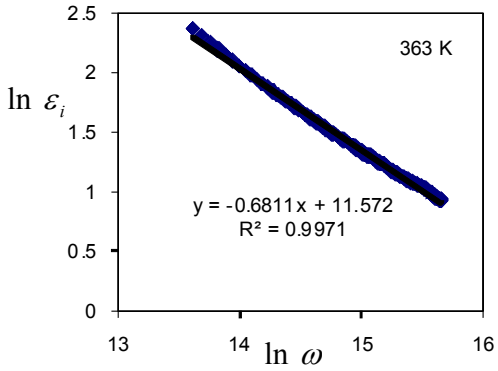

Figure 5.15 (*f*)

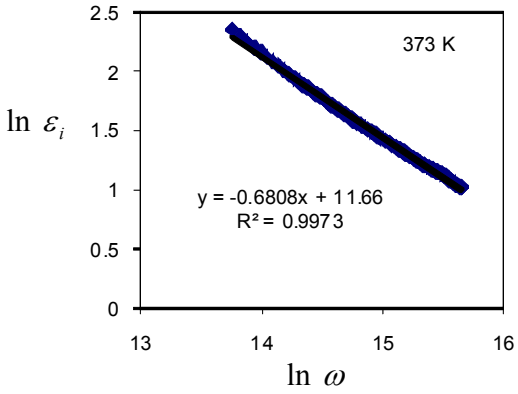

Figure 5.15 (*g*)

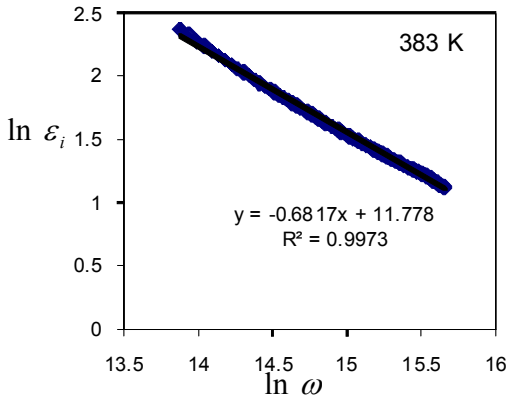

Figure 5.15 (*h*)

Continue …

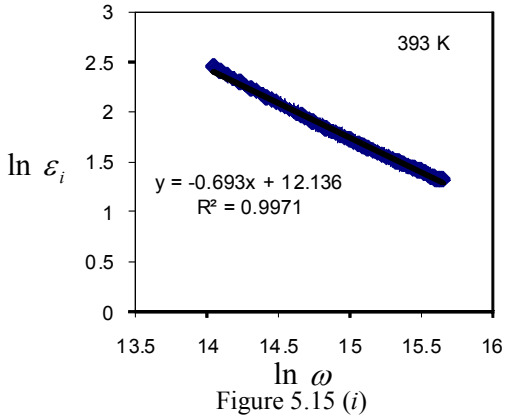

Figure 5.15 (*i*)

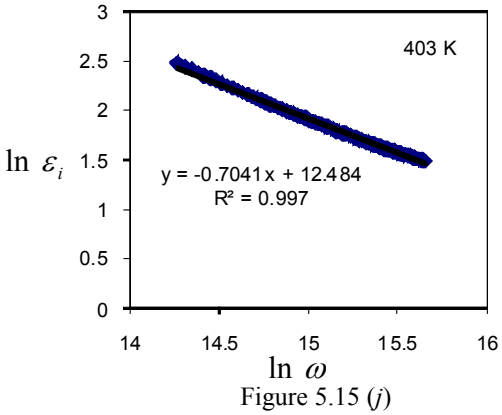

Figure 5.15 (*j*)

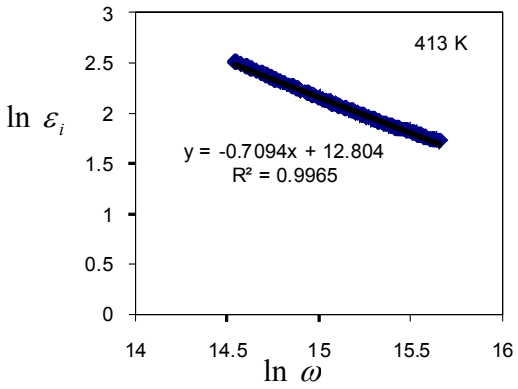

Figure 5.15 (*k*)

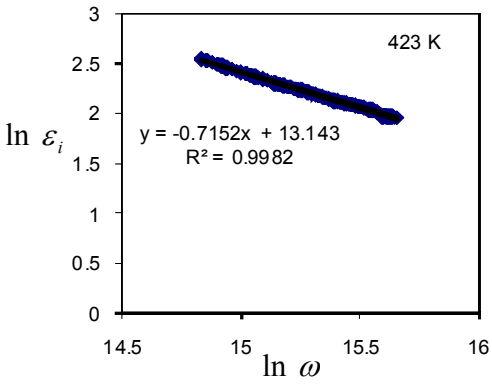

Figure 5.15 (*l*)

Figure 5.15: $\ln \varepsilon_i$ versus $\ln \omega$ (Hz) at various temperatures for 0.2CuI-0.8AgI.

For the 0.3CuI-0.7AgI sample, the graphs are depicted in Figure 5.16 (*a*) to 5.16 (*l*).

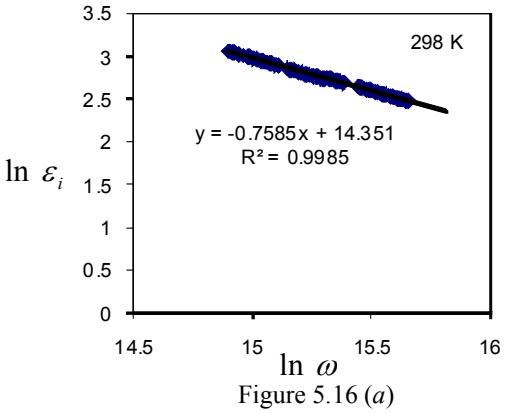

Figure 5.16 (*a*)

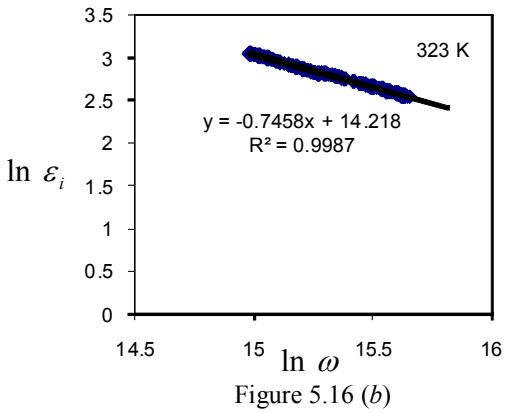

Figure 5.16 (*b*)

Continue …

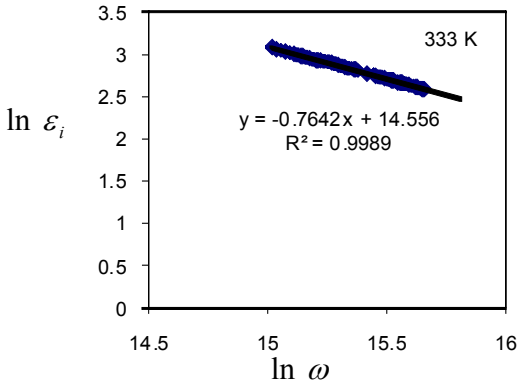

Figure 5.16 (*c*)

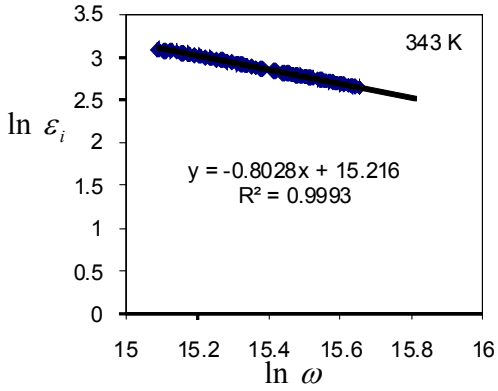

Figure 5.16 (*d*)

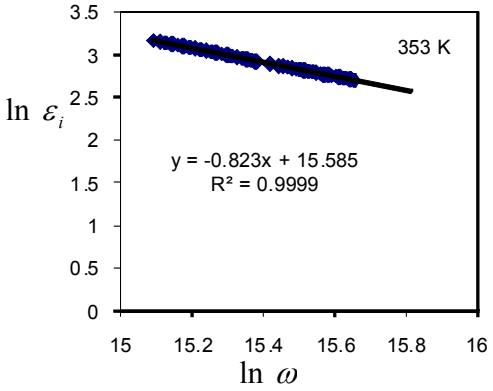

Figure 5.16 (*e*)

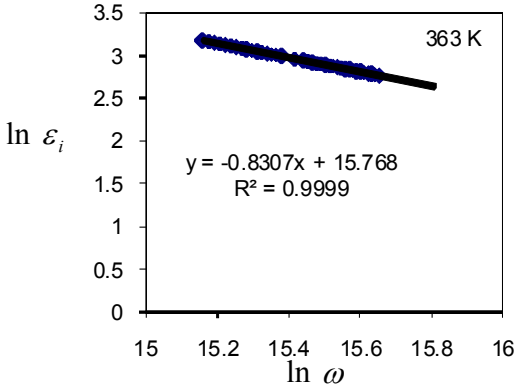

Figure 5.16 (*f*)

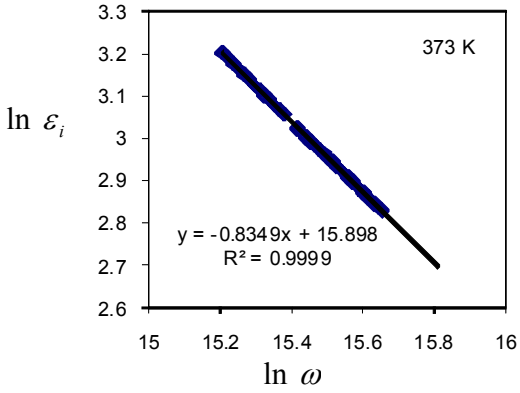

Figure 5.16 (*g*)

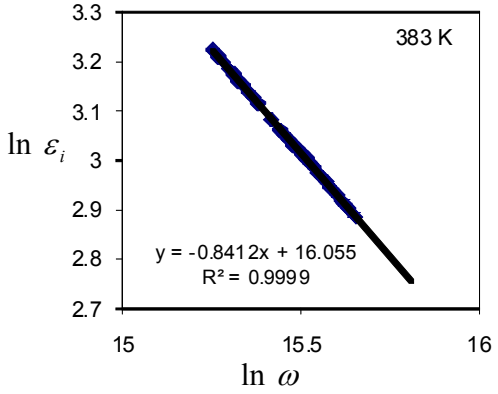

Figure 5.16 (*h*)

Continue …

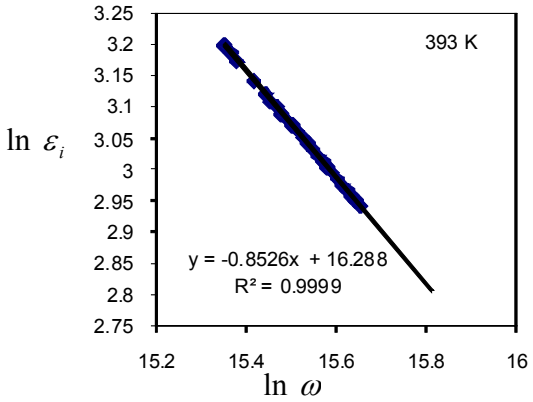

Figure 5.16 (*i*)

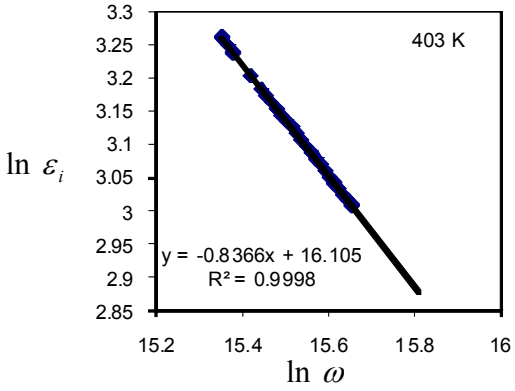

Figure 5.16 (*j*)

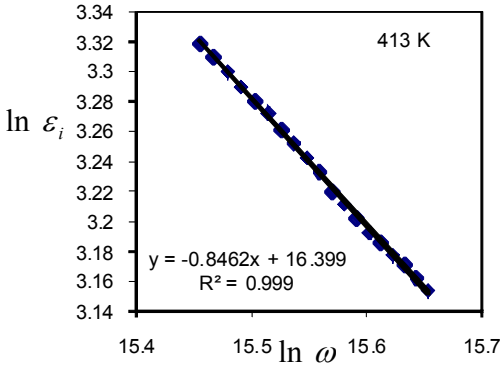

Figure 5.16 (*k*)

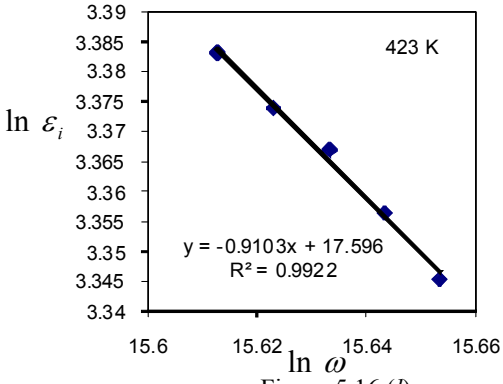

Figure 5.16 (*l*)

Figure 5.16: $\ln \varepsilon_i$ versus $\ln \omega$ (Hz) at various temperatures for 0.3CuI-0.7AgI.

For the 0.4CuI-0.6AgI sample, the graphs are depicted in Figure 5.17 (*a*) to 5.17 (*l*).

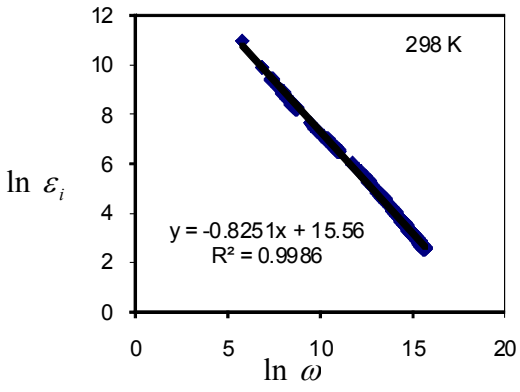

Figure 5.17 (*a*)

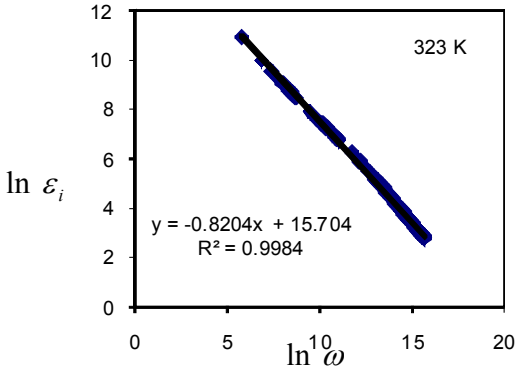

Figure 5.17 (*b*)

Continue …

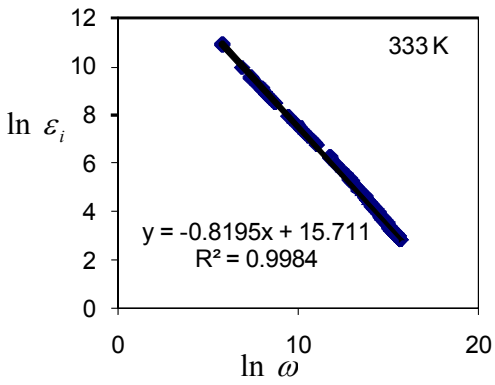

Figure 5.17 (*c*)

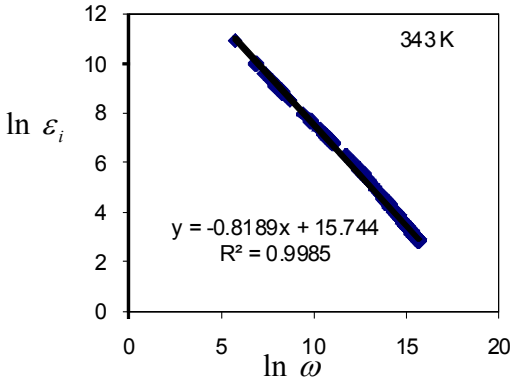

Figure 5.17 (*d*)

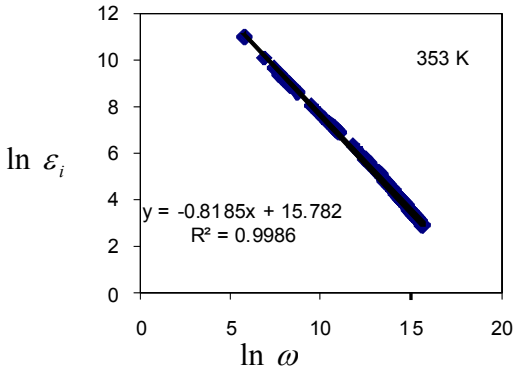

Figure 5.17 (*e*)

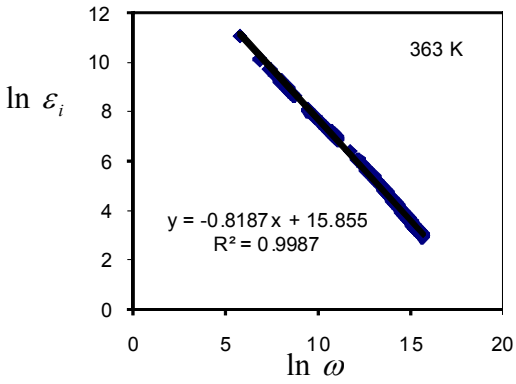

Figure 5.17 (*f*)

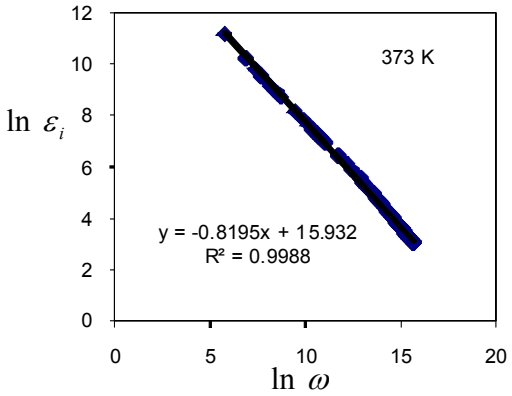

Figure 5.17 (*g*)

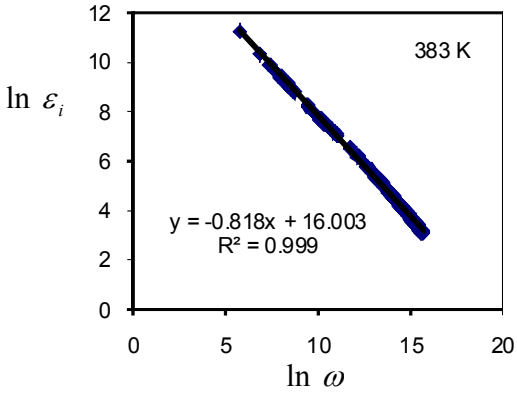

Figure 5.17 (*h*)

Continue …

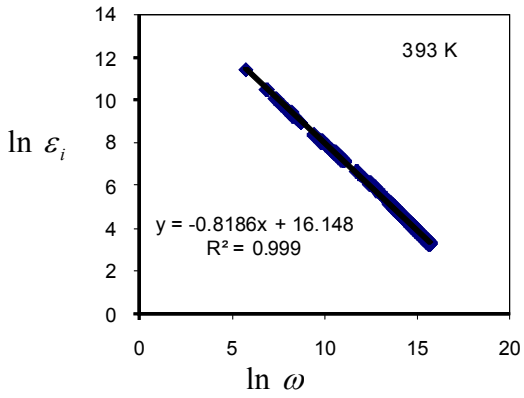

Figure 5.17 (*i*)

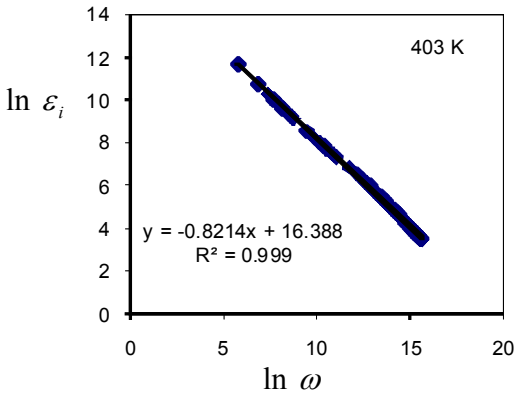

Figure 5.17 (*j*)

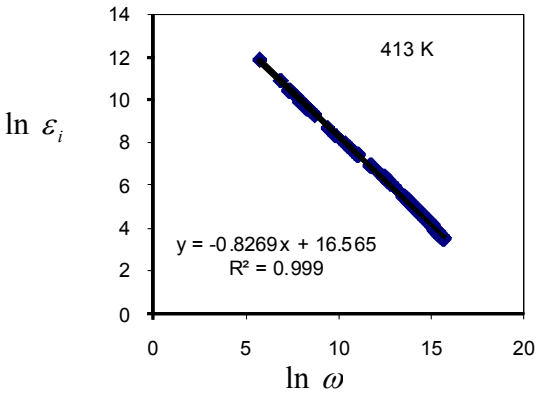

Figure 5.17 (*k*)

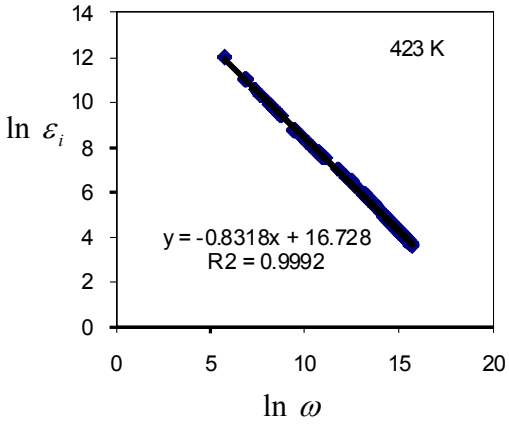

Figure 5.17 (*l*)

Figure 5.17: $\ln \varepsilon_i$ versus $\ln \omega$ (Hz) at 423 K for 0.4CuI-0.6AgI.

Figures above depict the frequency dependence of dielectric loss, ε_i at different temperatures. The value of exponent s can be obtained from the gradient of the graphs and is presented versus temperatures as in Figure 5.18 to Figure 5.22 for all samples.

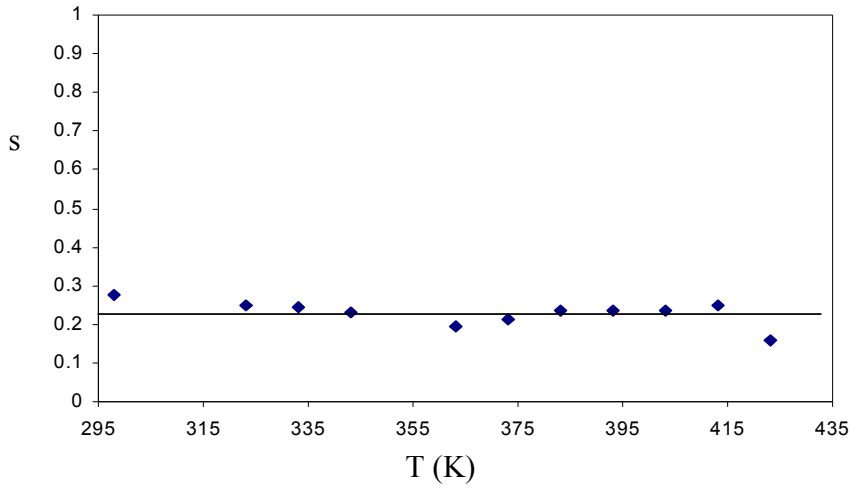

Figure 5.18: s versus T (K) for pure AgI.

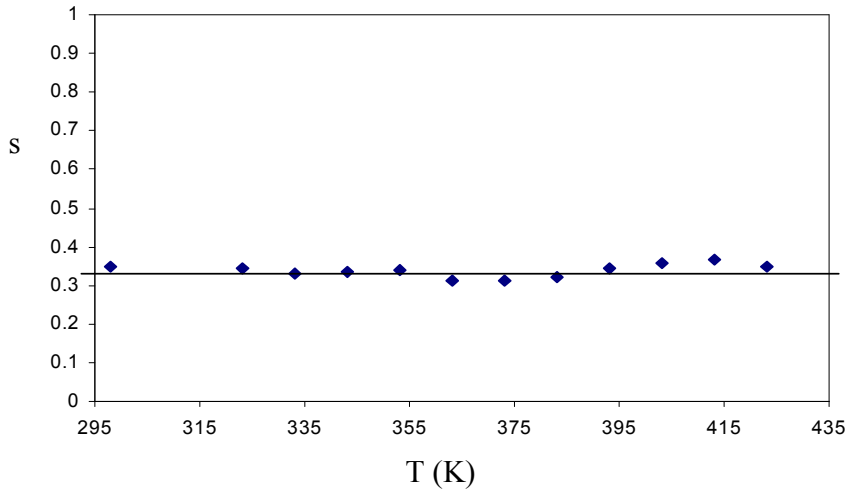

Figure 5.19: s versus T (K) for 0.1CuI-0.9AgI.

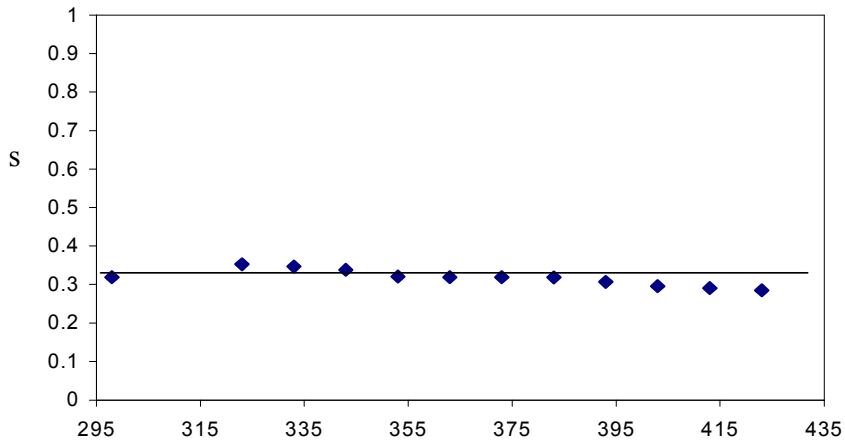

Figure 5.20: s versus T (K) for 0.2CuI-0.8AgI.

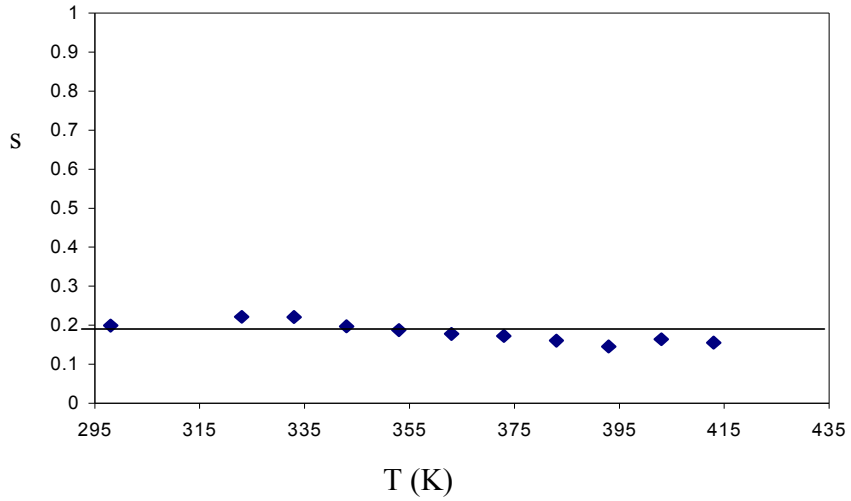

Figure 5.21: s versus T (K) for 0.3CuI-0.7AgI.

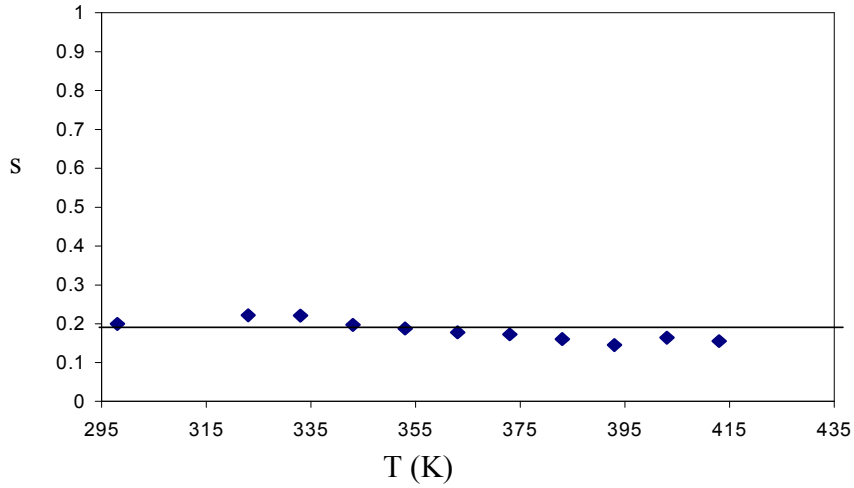

Figure 5.22: s versus T (K) for 0.4CuI-0.6AgI.

A number of theoretical models have been proposed to analyze the graphs of s versus T. In the quantum mechanical tunneling (QMT) model, the exponent or index s is independent of temperature. In the overlapping large polaron tunneling (OLPT) model, the exponent s is temperature dependent. In the OLPT model, the s decreases to a minimum value and increases again as the varied temperature increases. In the small polaron (SP) model, s has been observed to increase with increasing temperature. In the correlated

barrier hopping (CBH) model, s decreases with increasing temperature but there is no minimum value of s to be observed.

From the plot of s versus T for different compositions of AgI-CuI, the gradient of graph $x = 0$ is at -0.0004, gradient of graph $x = 0.1$ is at -0.0001, gradient of graph $x = 0.2$ is at -0.0005, gradient of graph $x = 0.3$ is at -0.0006 and gradient of graph $x = 0.4$ is at -0.0006. The slope is quite low indicating that the line is almost flat or is almost parallel to the horizontal axis. The almost flat nature of the trend line is an indication that the s depends very little in temperature and may be considered to be independent of temperature Therefore, it can be inferred that QMT model is more applicable in explaining the conduction mechanism in the AgI-CuI system prepared by sintering the mixture at 250^0C for 5 hours.

5.5 Modulus Studies

According to Ganguli et.al (1999), it is appropriate to examine the dielectric data using the modulus representation which suppresses the d.c polarization effect. Further analysis of the dielectric behavior in the modulus formalism was also carried out in this work. The real, M_r and the imaginary, M_i parts of electrical modulus for the samples xCuI-(1-x)AgI, ($0 \leq x \leq 0.4$) is shown in Figure 5.23 and Figure 5.24.

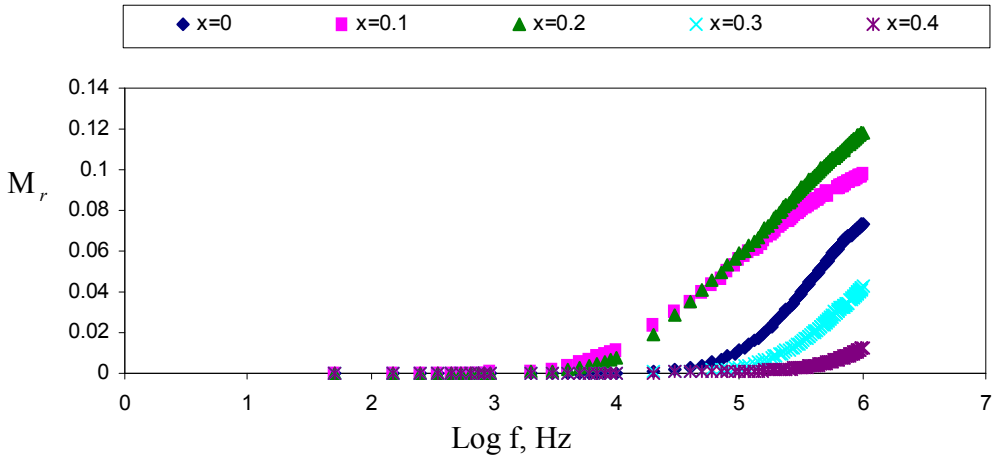

Figure 5.23: Plots of variation of real (M_r) modulus constant as a function of frequency for AgI-CuI at different compositions.

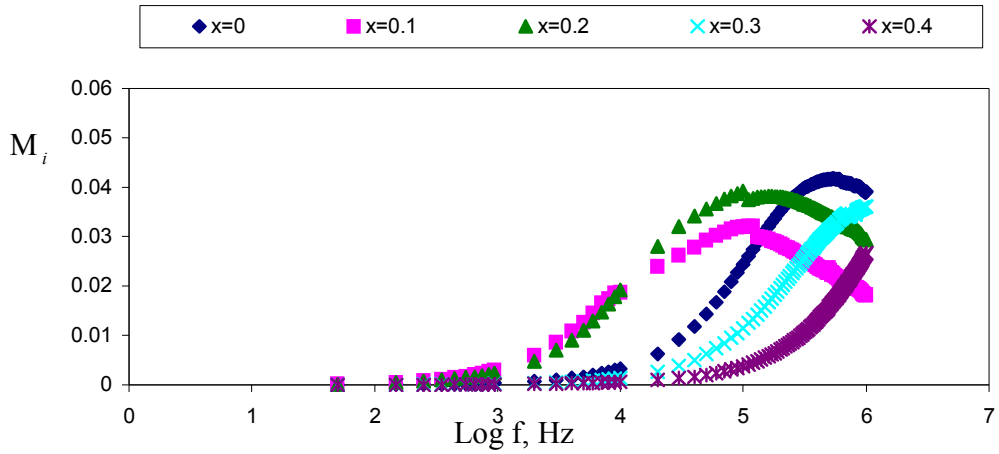

Figure 5.24: Plots of variation of imaginary (M_i) modulus constant as a function of frequency for AgI-CuI at different compositions.

In Figure 5.23, there is no peak observed. This maybe due to the possibility of the relaxation peak occurring at frequencies higher than the range permitted by the instrument used. It can also be observed that the height of the peak was not constant at various weight percentage of the AgI-CuI mixture. Therefore, there maybe not is a single relaxation mechanism operating in these samples (Ganguli et.al, 1999).

The electrical modulus in Figure 5.24 increases as the conductivity decreases since $M^* = \frac{1}{\varepsilon^*}$ where M^* is the complex electrical modulus and ε^* is the complex permittivity. The presence of a relaxation peak towards the high frequency region in the modulus-frequency plot indicates that the samples are ionic conductor (Mellander and Albinsson, 1996). M_r and M_i approaches zero at low frequencies. A long tail at lower frequencies can also be observed in the plots. This long tail is due to the large capacitance associated with the electrodes.

The behavior of the imaginary and the real parts of the modulus for the sample containing different weight percent of AgI-CuI mixture at different temperatures has also been studied. Figures below show the variation of the real (M_r) and the imaginary (M_i) part with frequency.

5.5.1 Variation of M_r with frequency at different temperatures for *x*CuI-(1-*x*)AgI, $(0 \leq x \leq 0.4)$

M_r versus frequency for AgI at temperatures investigated are shown in Figure 5.25 (*a*) to 5.25 (*l*).

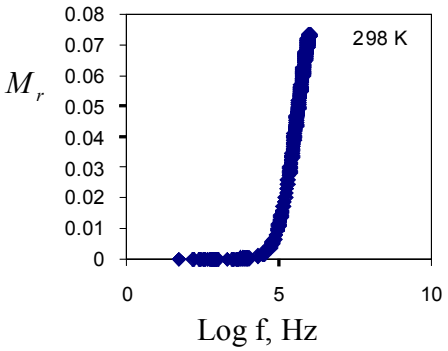

Figure 5.25 (*a*)

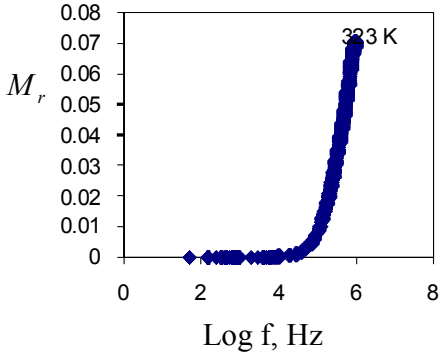

Figure 5.25 (*b*)

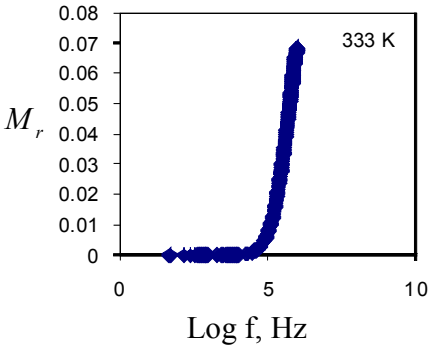

Figure 5.25 (*c*)

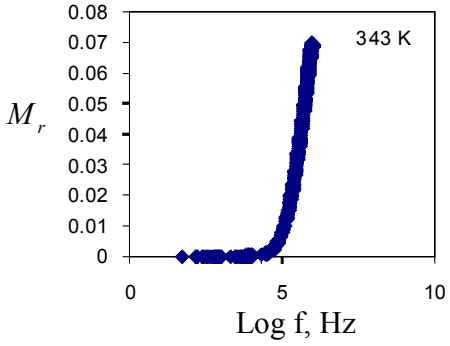

Figure 5.25 (*d*)

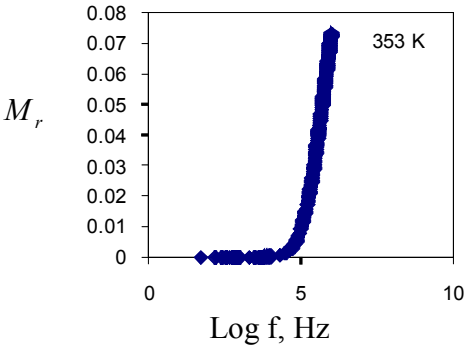

Figure 5.25 (*e*)

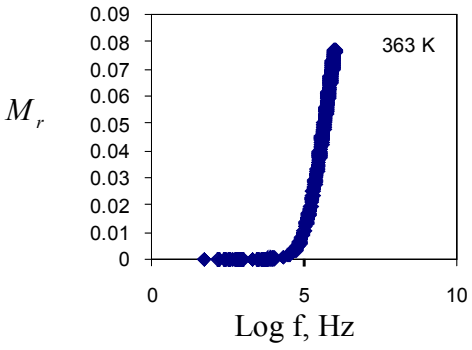

Figure 5.25 (*f*)

Continue …

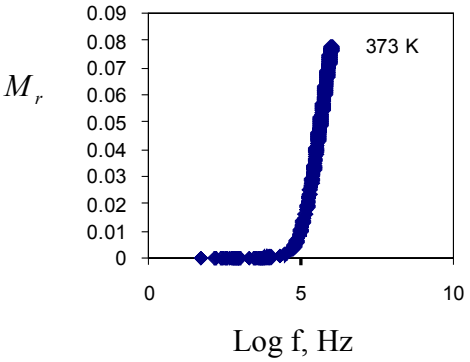

Figure 5.25 (*g*)

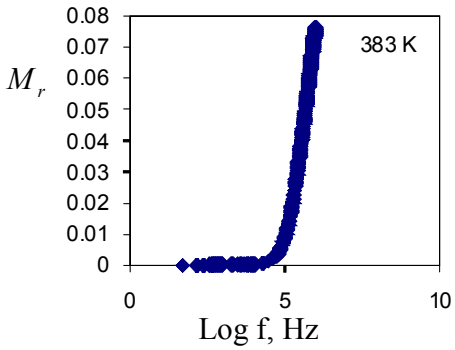

Figure 5.25 (*h*)

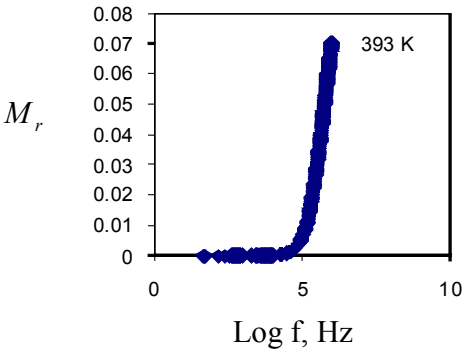

Figure 5.15 (*i*)

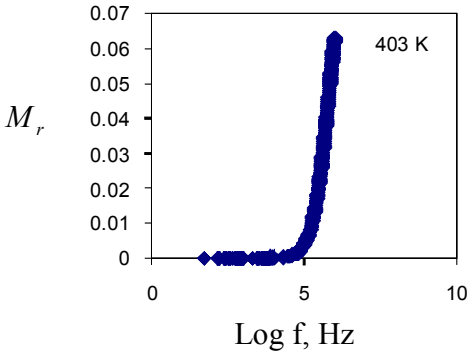

Figure 5.15 (*j*)

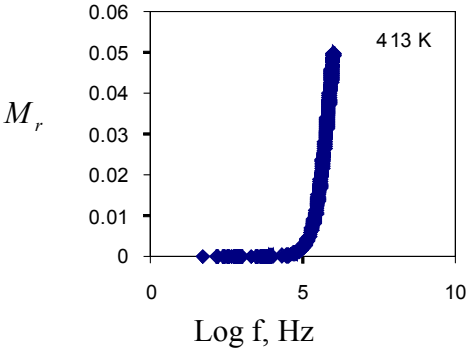

Figure 5.25 (*k*)

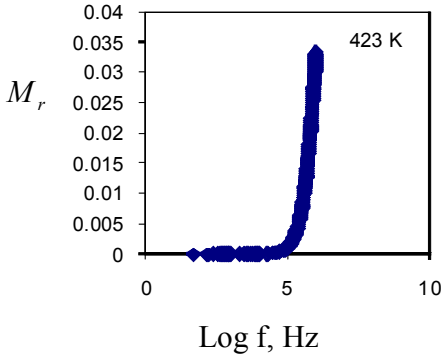

Figure 5.25 (*l*)

Figure 5.25: Plots of real part of modulus with frequency at several temperatures for pure AgI.

M_r versus frequency for 0.1CuI-0.9AgI at temperatures investigated are shown in Figure 5.26 (*a*) to 5.26 (*l*).

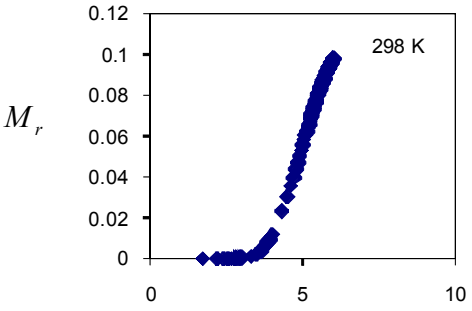

Figure 5.26 (*a*)

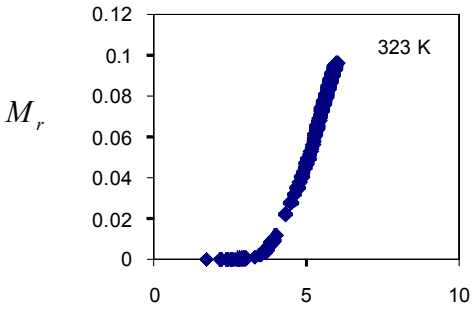

Figure 5.26 (*b*)

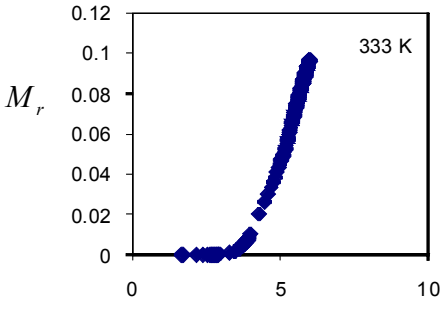

Figure 5.26 (*c*)

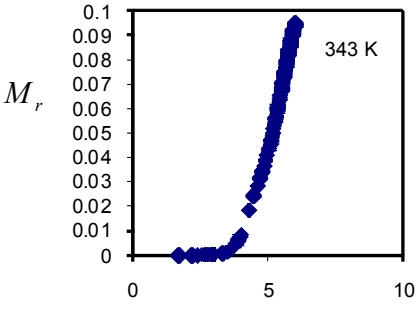

Figure 5.26 (*d*)

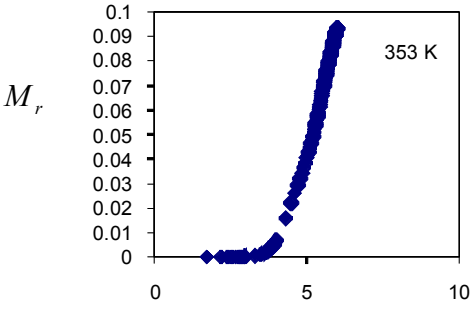

Figure 5.26 (*e*)

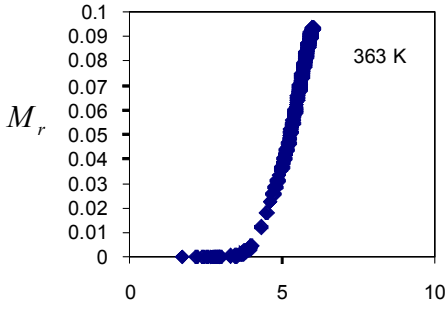

Figure 5.26 (*f*)

Continue …

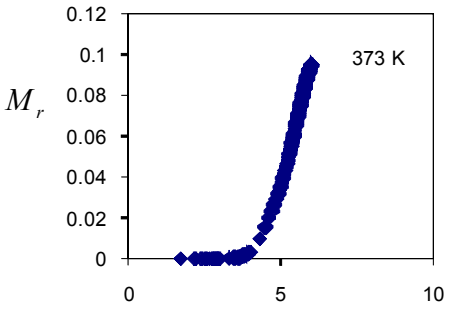

Figure 5.26 (*g*)

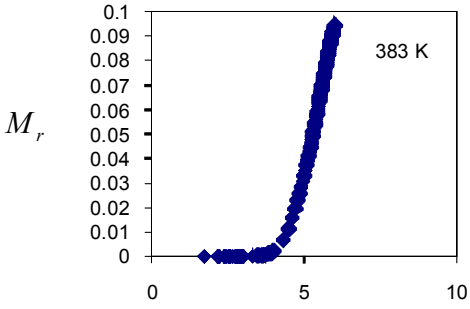

Figure 5.26 (*h*)

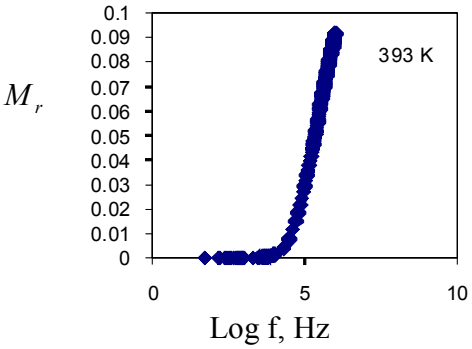

Figure 5.16 (*i*)

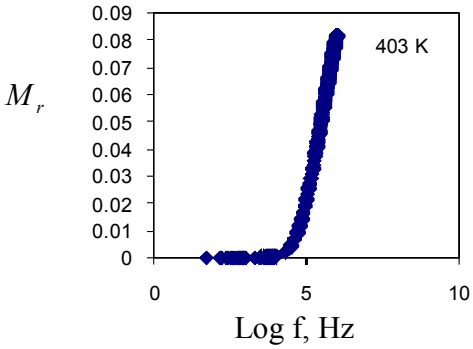

Figure 5.16 (*j*)

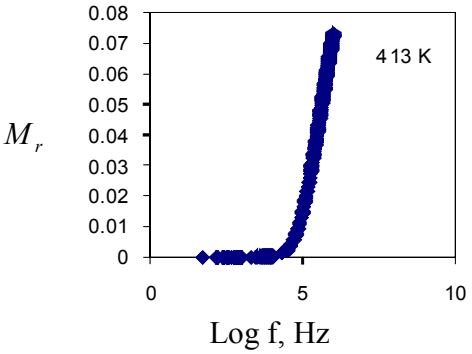

Figure 5.26 (*k*)

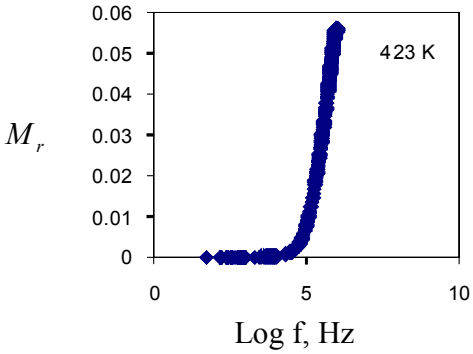

Figure 5.26 (*l*)

Figure 5.26: Plots of real part of modulus with frequency at several temperatures for 0.1CuI-0.9AgI.

M_r versus frequency for 0.2CuI-0.8AgI at temperatures investigated are shown in Figure 5.27 (*a*) to 5.27 (*l*).

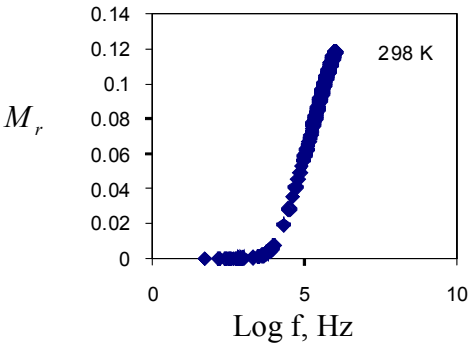

Figure 5.27 (*a*)

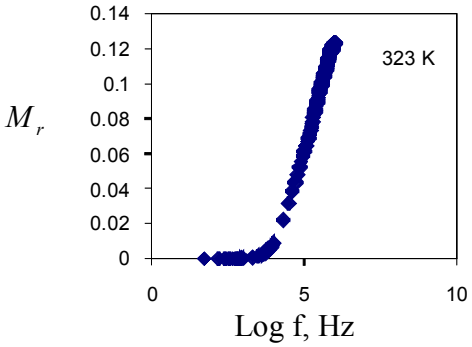

Figure 5.27 (*b*)

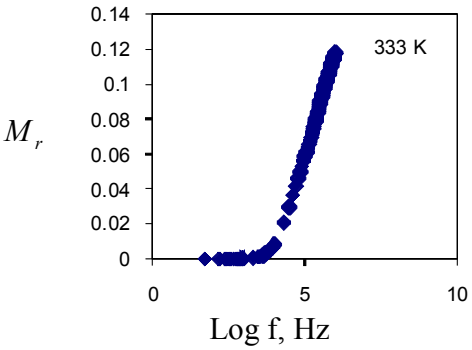

Figure 5.27 (*c*)

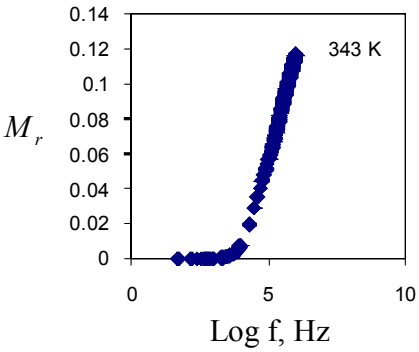

Figure 5.27 (*d*)

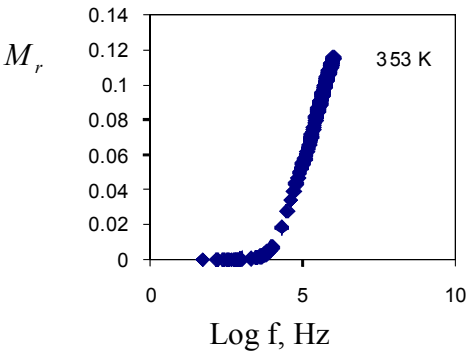

Figure 5.27 (*e*)

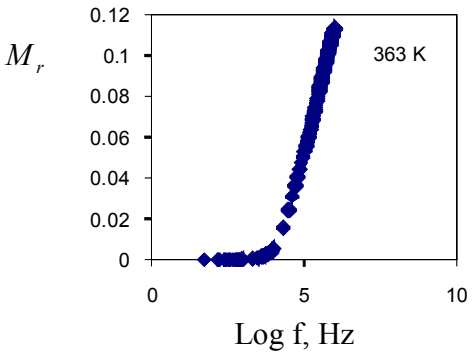

Figure 5.27 (*f*)

Continue …

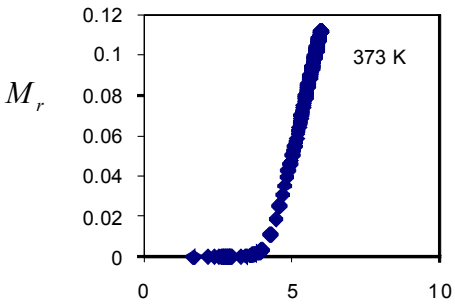

Figure 5.27 (*g*)

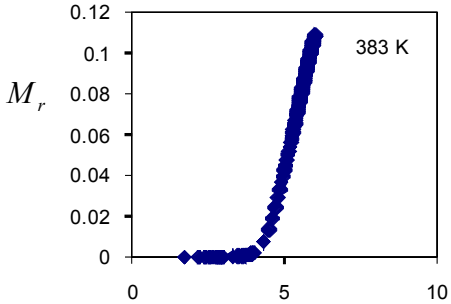

Figure 5.27 (*h*)

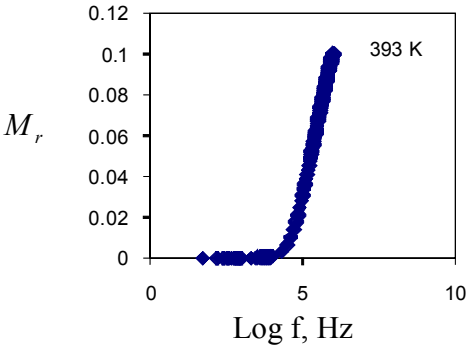

Figure 5.27 (*i*)

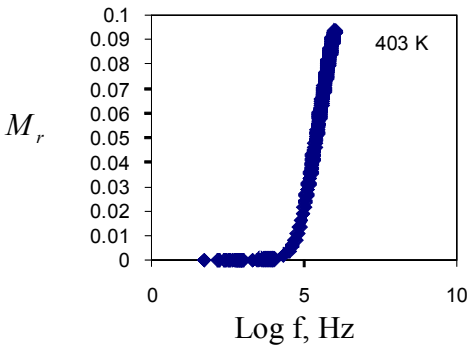

Figure 5.27 (*j*)

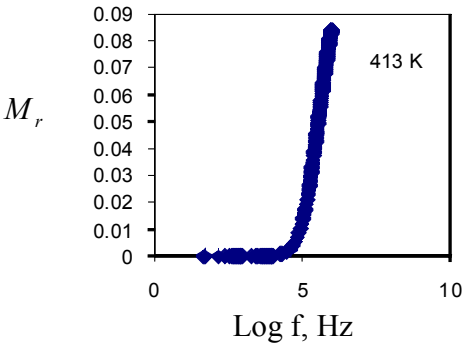

Figure 5.27 (*k*)

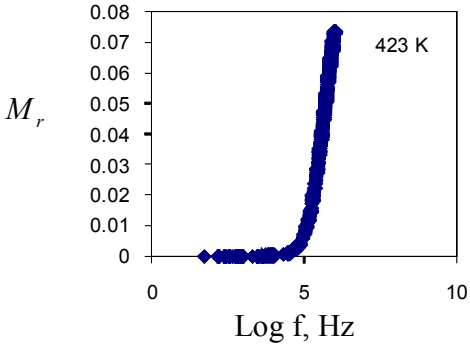

Figure 5.27 (*l*)

Figure 5.27: Plots of real part of modulus with frequency at several temperatures for 0.2CuI-0.8AgI.

M_r versus frequency for 0.3CuI-0.7AgI at temperatures investigated are shown in Figure 5.28 (*a*) to 5.28 (*l*).

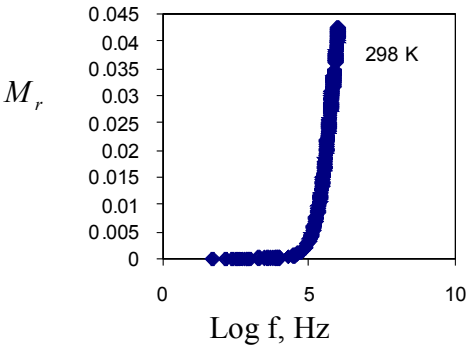

Figure 5.28 (*a*)

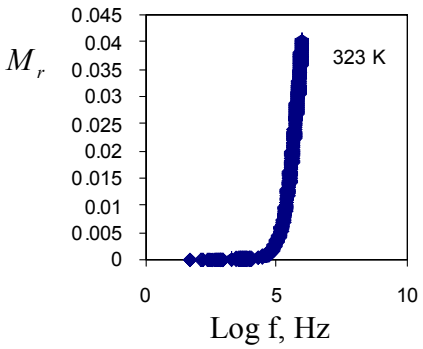

Figure 5.28 (*b*)

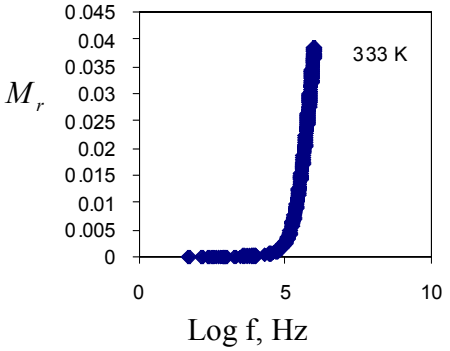

Figure 5.28 (*c*)

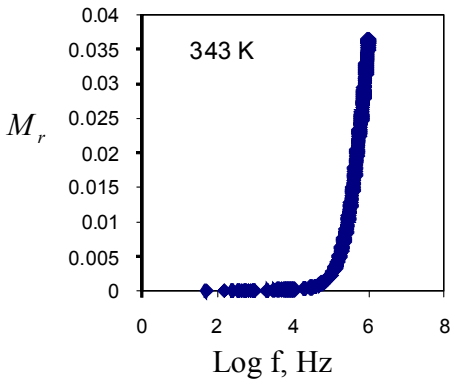

Figure 5.28 (*d*)

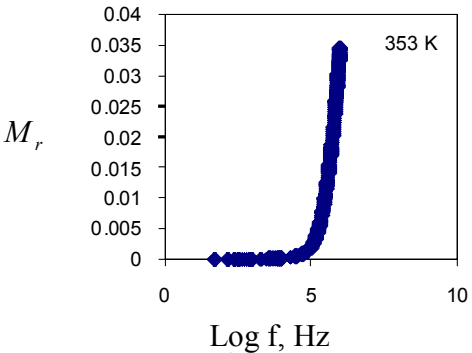

Figure 5.28 (*e*)

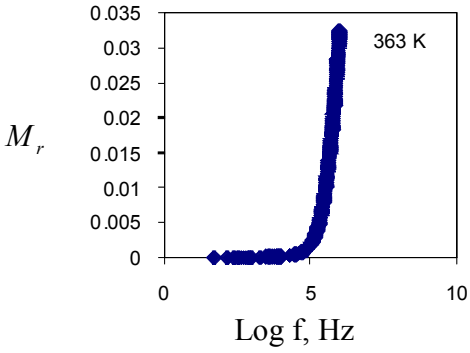

Figure 5.28 (*f*)

Continue …

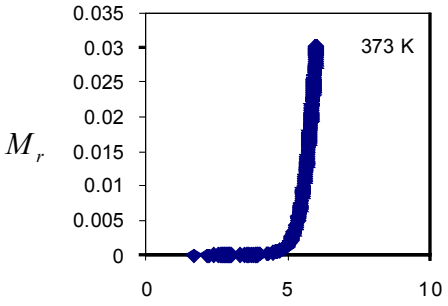

Figure 5.28 (*g*)

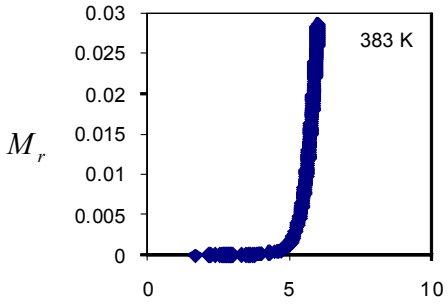

Figure 5.28 (*h*)

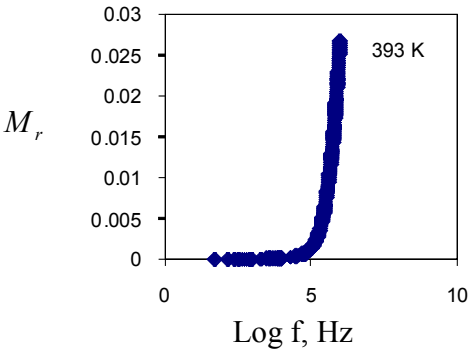

Figure 5.28 (*i*)

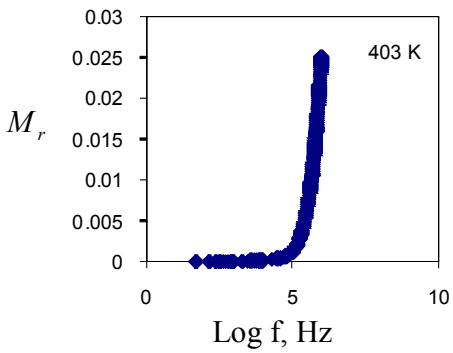

Figure 5.28 (*j*)

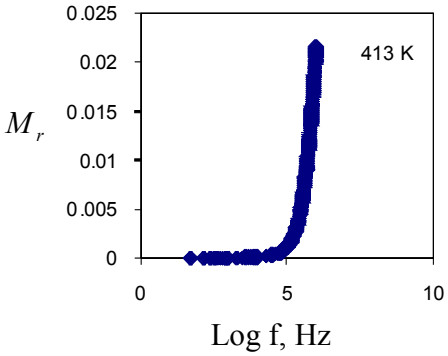

Figure 5.28 (*k*)

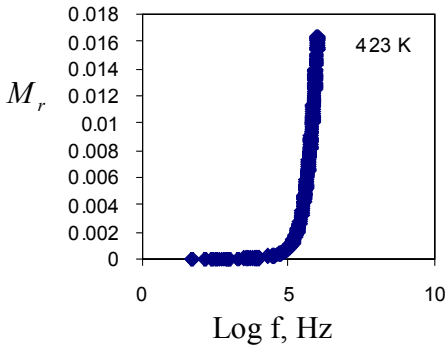

Figure 5.28 (*l*)

Figure 5.28: Plots of real part of modulus with frequency at several temperatures for 0.3CuI-0.7AgI.

M_r versus frequency for 0.4CuI-0.6AgI at temperatures investigated are shown in Figure 5.29 (*a*) to 5.29 (*l*).

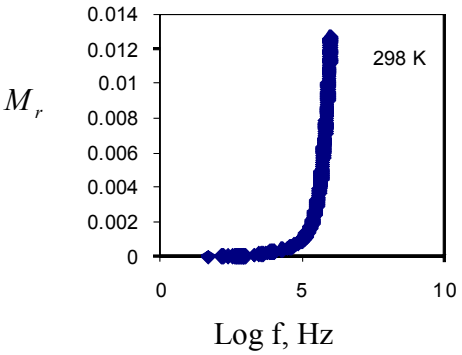

Figure 5.29 (*a*)

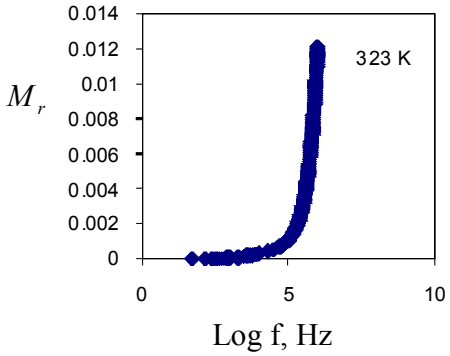

Figure 5.29 (*b*)

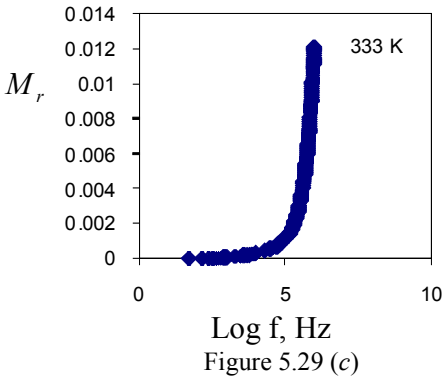

Figure 5.29 (*c*)

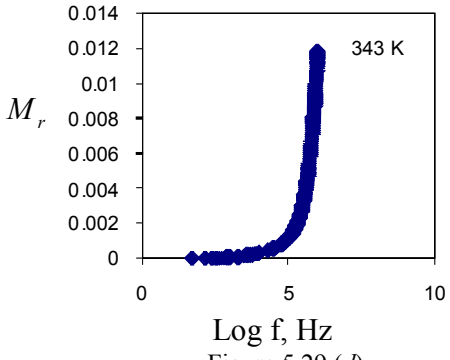

Figure 5.29 (*d*)

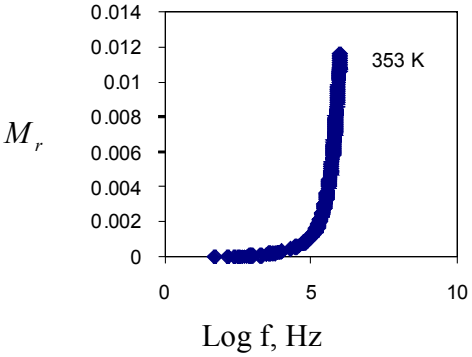

Figure 5.29 (*e*)

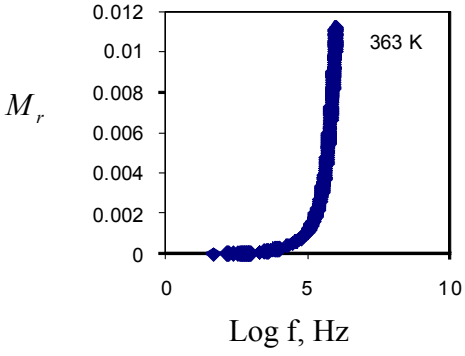

Figure 5.29 (*f*)

Continue …

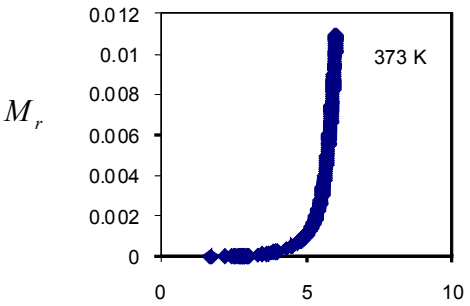

Figure 5.29 (*g*)

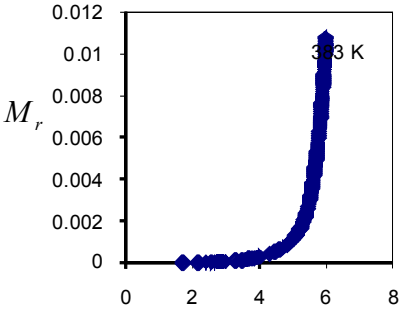

Figure 5.29 (*h*)

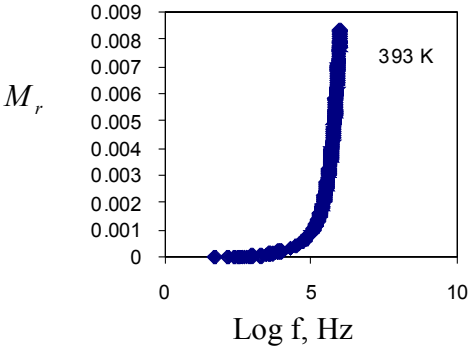

Figure 5.29 (*i*)

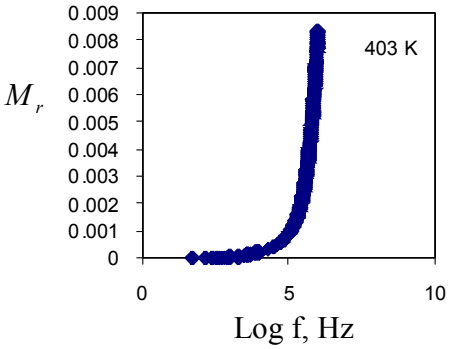

Figure 5.29 (*j*)

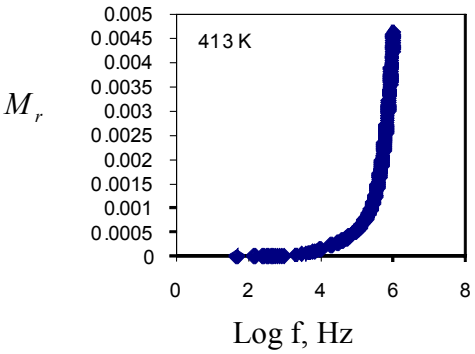

Figure 5.29 (*k*)

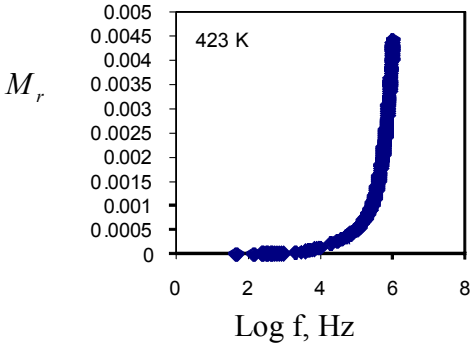

Figure 5.29 (*l*)

Figure 5.29: Plots of real part of modulus with frequency at several temperatures for 0.4CuI-0.6AgI.

There are no peaks observed for all M_r variations with frequency for all xCuI-(1-x)AgI, $(0 \leq x \leq 0.4)$.

5.5.2 Variation of M_i with frequency at different temperatures for *x*CuI-(1-*x*)AgI, $(0 \leq x \leq 0.4)$

M_i versus frequency for AgI at temperatures investigated are shown in Figure 5.30 (*a*) to 5.30 (*l*).

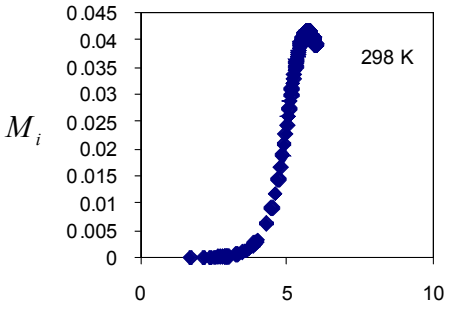

Figure 5.30 (*a*)

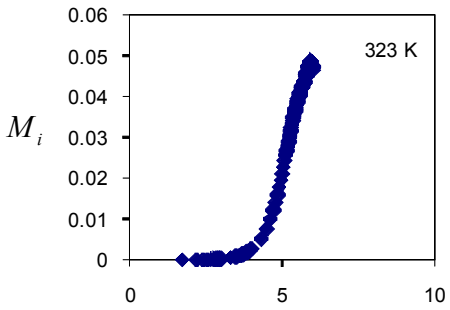

Figure 5.30 (*b*)

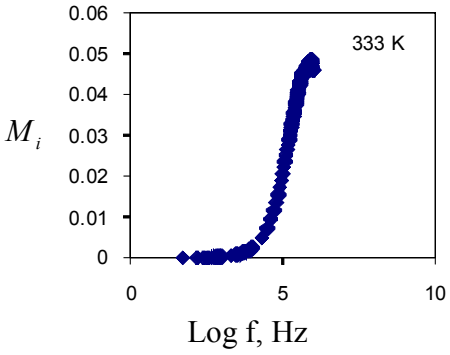

Figure 5.30 (*c*)

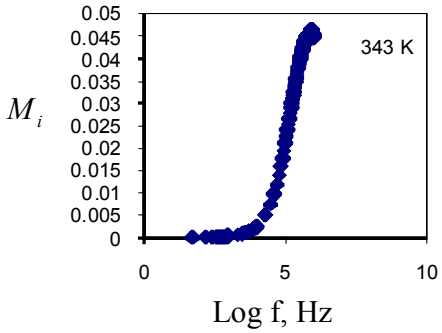

Figure 5.30 (*d*)

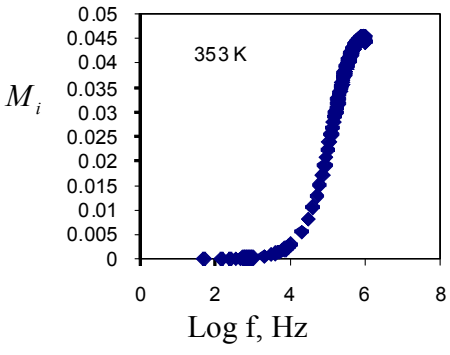

Figure 5.30 (*e*)

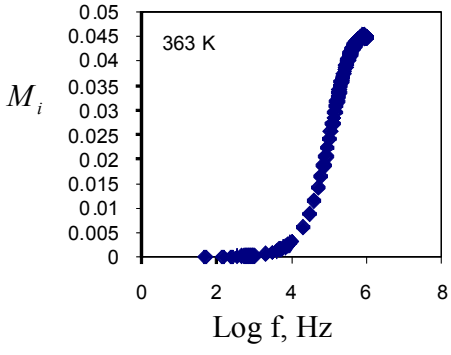

Figure 5.30 (*f*)

Continue …

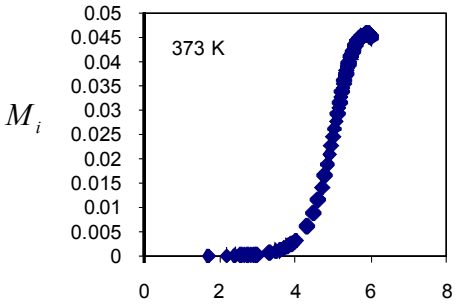

Figure 5.30 (*g*)

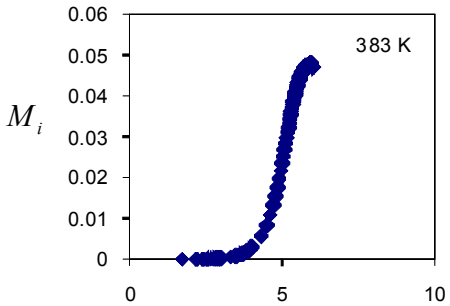

Figure 5.30 (*h*)

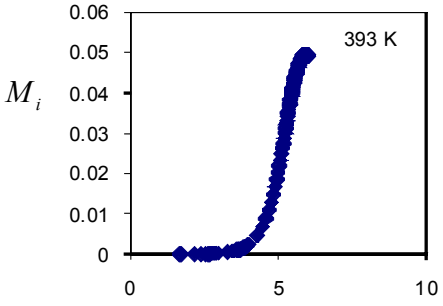

Figure 5.30 (*i*)

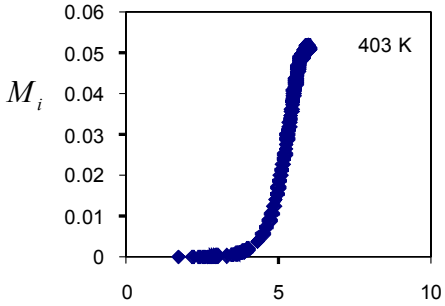

Figure 5.30 (*j*)

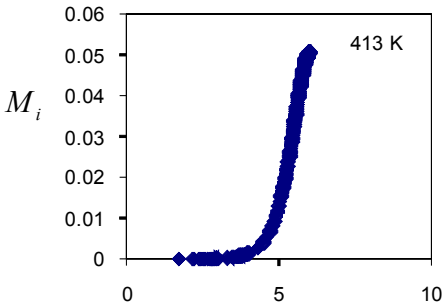

Figure 5.30 (*k*)

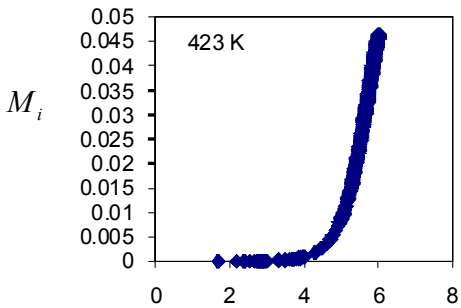

Figure 5.30 (*l*)

Figure 5.30: Plots of imaginary part of modulus with frequency at several temperatures for pure AgI.

The peak frequency for pure AgI change from 336 kHz (298 K) to 1000 kHz (323 K), to 631 kHz (333 K, 343 K and 353 K), to 100 kHz (363 K), to 631 kHz (373 K and 383 K), to 1000 kHz (393 K, 403 K and 413 K), to 1580 kHz (423 K).

M_i versus frequency for 0.1CuI-0.9AgI at temperatures investigated are shown in Figure 5.31 (*a*) to 5.31 (*l*).

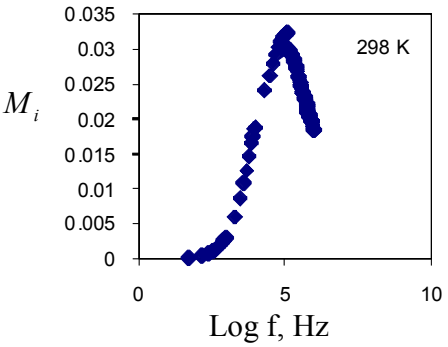

Figure 5.31 (*a*)

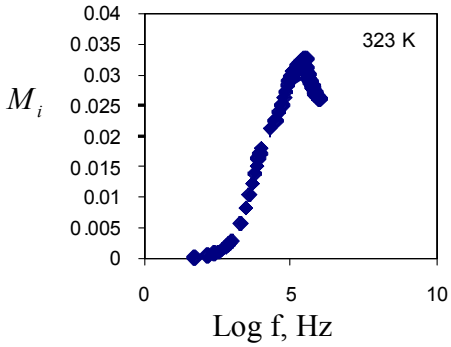

Figure 5.31 (*b*)

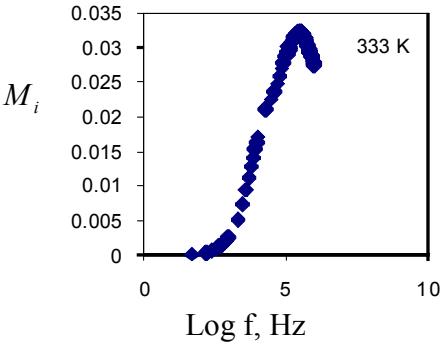

Figure 5.31 (*c*)

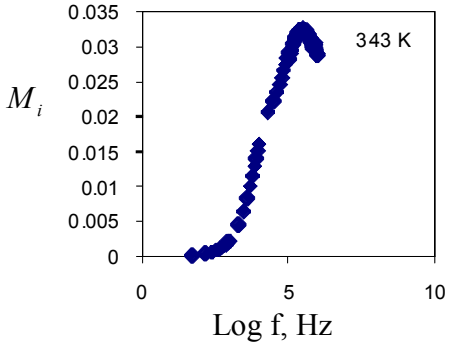

Figure 5.31 (*d*)

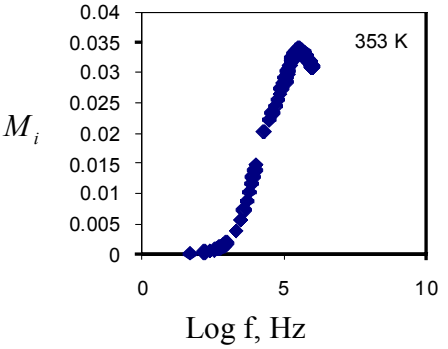

Figure 5.31 (*e*)

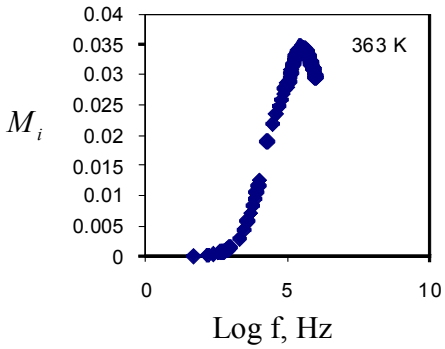

Figure 5.31 (*f*)

Continue …

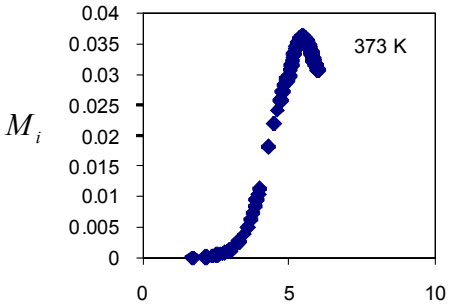

Figure 5.31 (*g*)

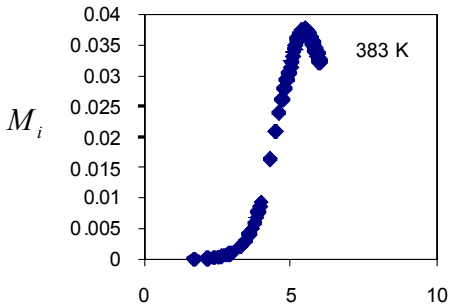

Figure 5.31 (*h*)

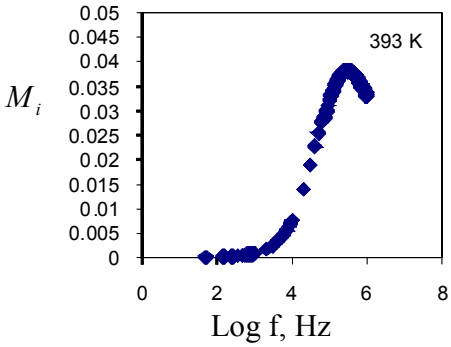

Figure 5.31 (*i*)

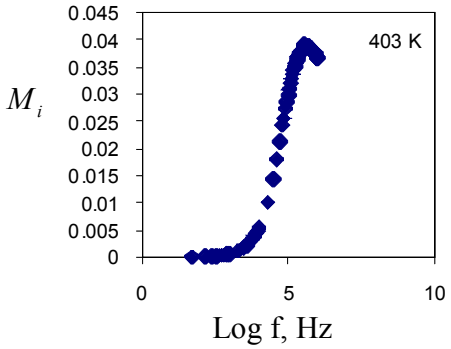

Figure 5.31 (*j*)

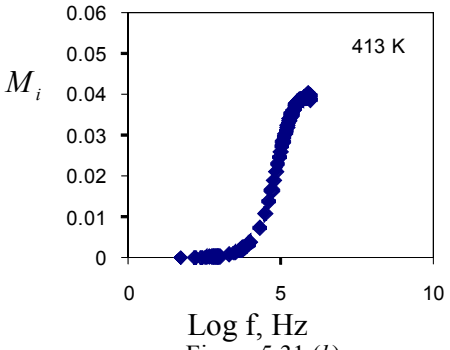

Figure 5.31 (*k*)

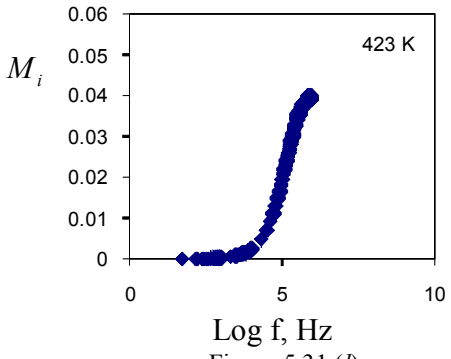

Figure 5.31 (*l*)

Figure 5.31: Plots of imaginary part of modulus with frequency at several temperatures for 0.1CuI-0.9AgI.

The peak frequency for 0.1CuI-0.9AgI change from 100 kHz (298 K) to 251 kHz (323 K), to 398 kHz (333 K and 343 K), to 359 kHz (353 K), to 251 kHz (363 K and 373 K), to 398 kHz (383 K), to 251 kHz (393 K), 398 kHz (403 K and 413 K), to 631 kHz (423 K).

M_i versus frequency for 0.2CuI-0.8AgI at temperatures investigated are shown in Figure 5.32 (*a*) to 5.32 (*l*).

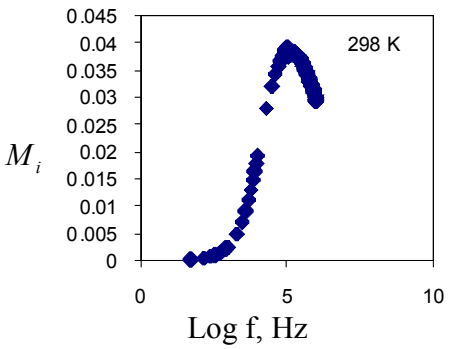

Figure 5.32 (*a*)

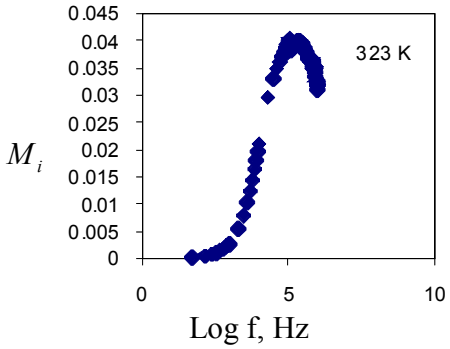

Figure 5.32 (*b*)

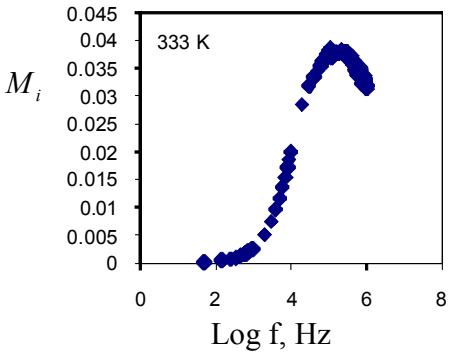

Figure 5.32 (*c*)

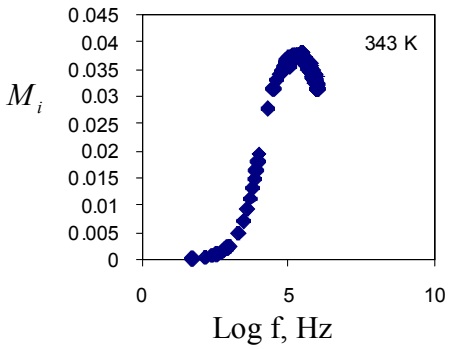

Figure 5.32 (*d*)

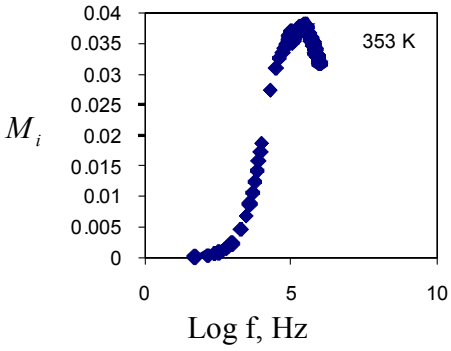

Figure 5.32 (*e*)

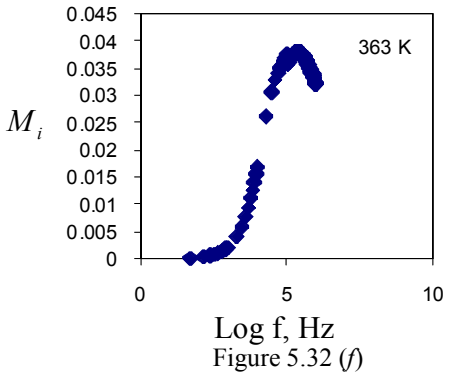

Figure 5.32 (*f*)

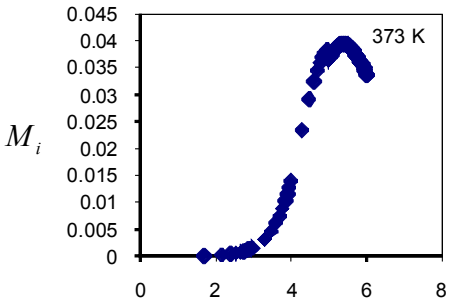

Figure 5.32 (*g*)

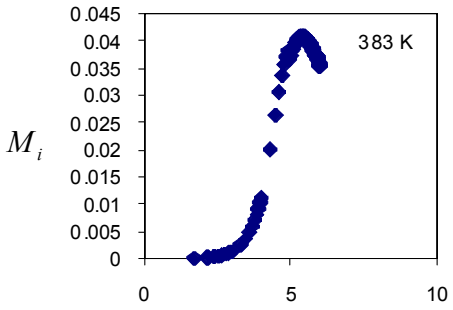

Figure 5.32 (*h*)

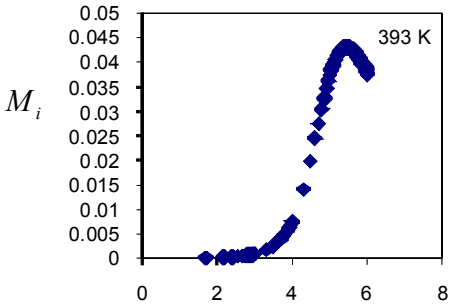

Figure 5.32 (*i*)

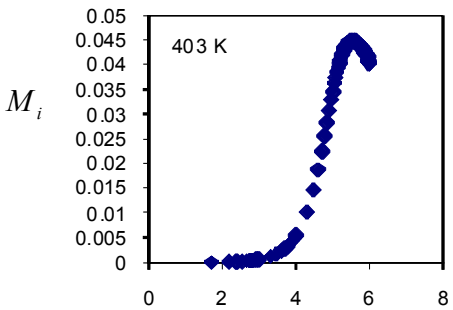

Figure 5.32 (*j*)

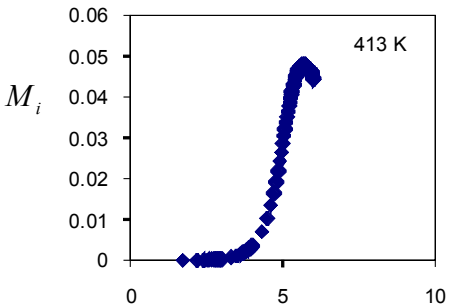

Figure 5.32 (*k*)

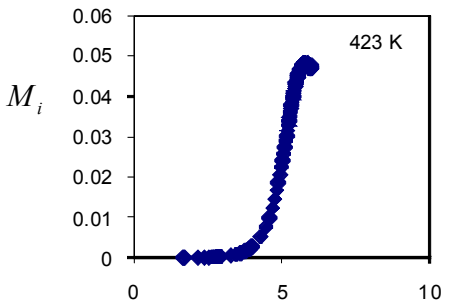

Figure 5.32 (*l*)

Figure 5.32: Plots of imaginary part of modulus with frequency at several temperatures for 0.2CuI-0.8AgI.

The peak frequency for 0.2CuI-0.8AgI change from 100 kHz (298 K) to 148 kHz (323 K and 333 K), to 251 kHz (343 K, 353 K, 363 K, 373 K, 383 K and 393 K), to 599 kHz (403 K), to 398 kHz (413 K) and to 631 kHz (423 K)

M_i versus frequency for 0.3CuI-0.7AgI at temperatures investigated are shown in Figure 5.33 (*a*) to 5.33 (*l*).

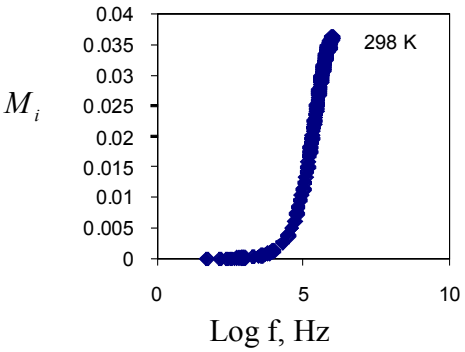

Figure 5.33 (*a*)

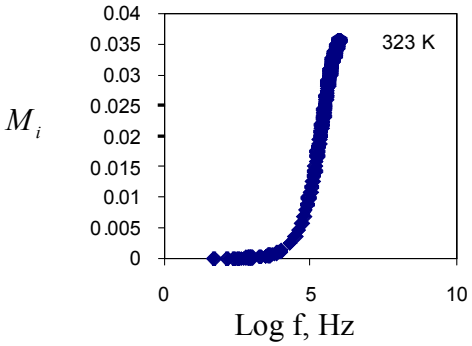

Figure 5.33 (*b*)

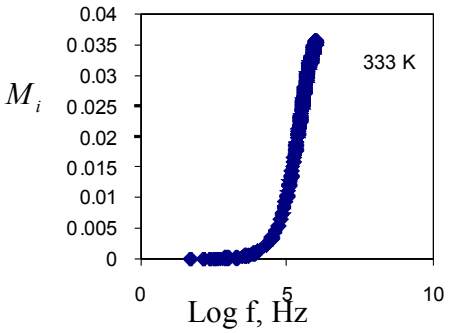

Figure 5.33 (*c*)

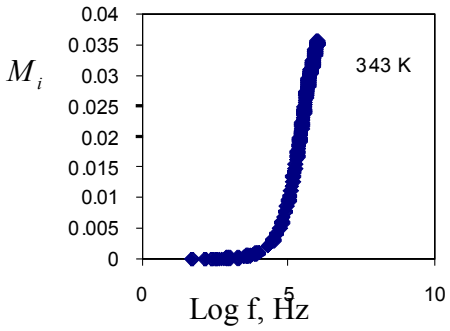

Figure 5.33 (*d*)

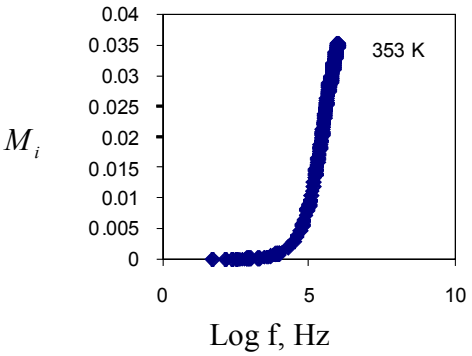

Figure 5.33 (e)

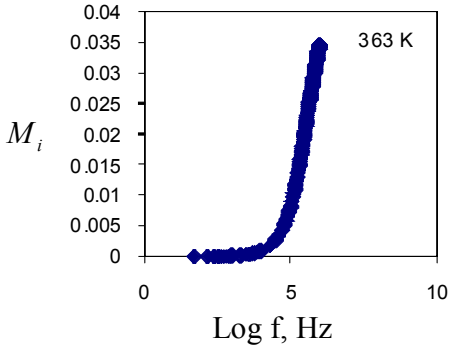

Figure 5.33 (*f*)

Continue …

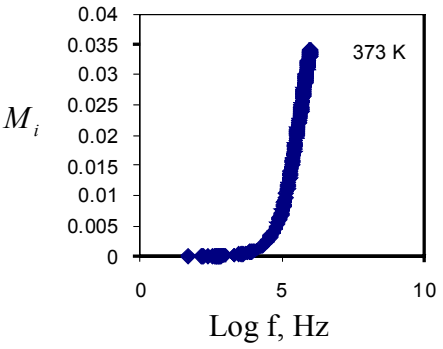

Figure 5.33 (*g*)

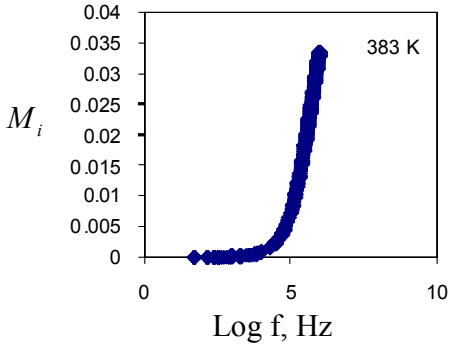

Figure 5.33 (*h*)

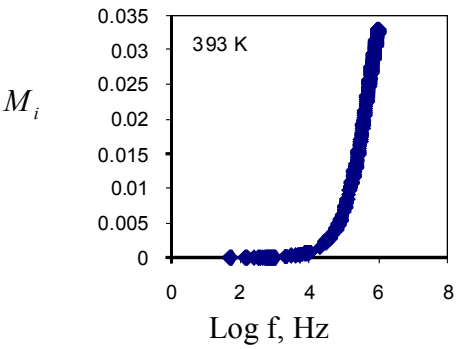

Figure 5.33 (*i*)

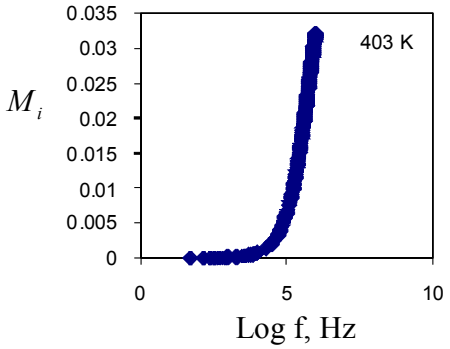

Figure 5.33 (*j*)

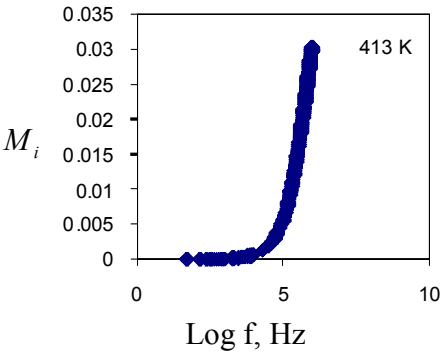

Figure 5.33 (*k*)

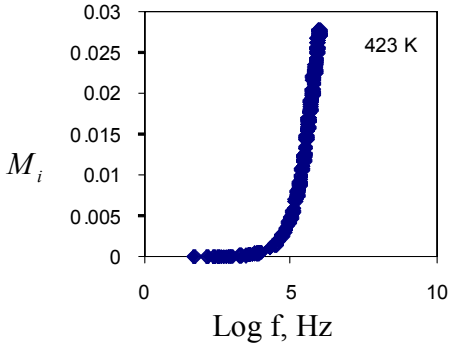

Figure 5.33 (*l*)

Figure 5.33: Plots of imaginary part of modulus with frequency at several temperatures for 0.3CuI-0.7AgI.

Unlike for previous samples, no peak was observed for 0.3CuI-0.7AgI sample in the temperature range investigated. The incorporation of 30 wt% CuI could have trasformed the CuI-AgI sample from pure ionic conductor to a mixed conductor.

M_i versus frequency for 0.4CuI-0.6AgI at temperatures investigated are shown in Figure 5.34 (*a*) to 5.34 (*l*).

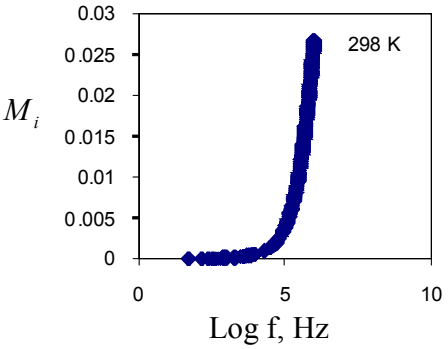

Figure 5.34 (*a*)

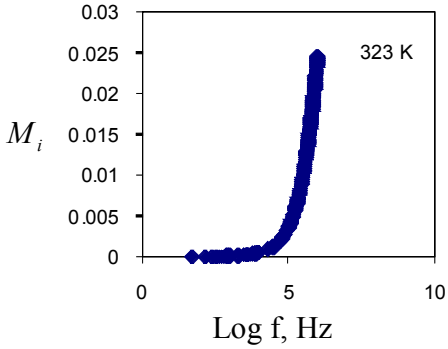

Figure 5.34 (*b*)

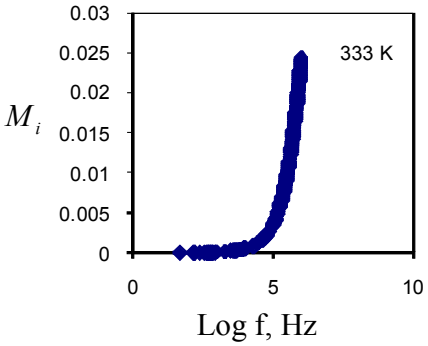

Figure 5.34 (*c*)

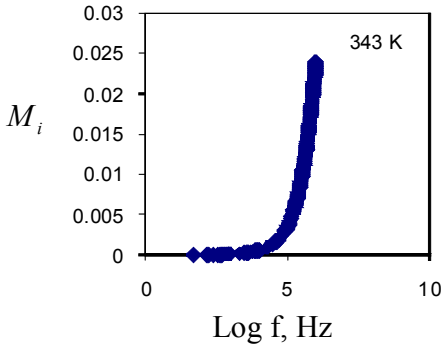

Figure 5.34 (*d*)

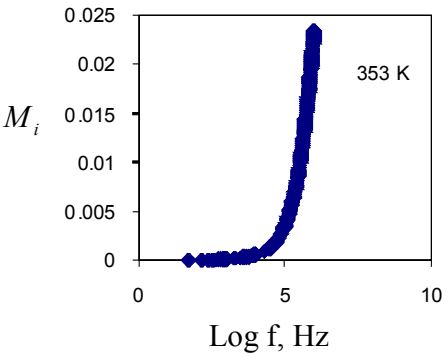

Figure 5.34 (*e*)

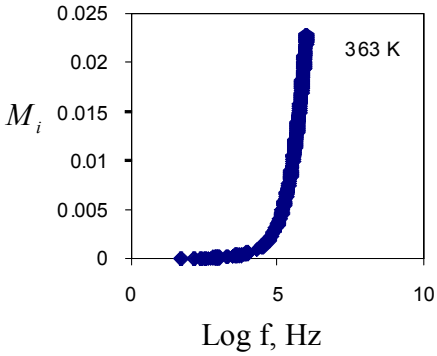

Figure 5.34 (*f*)

Continue …

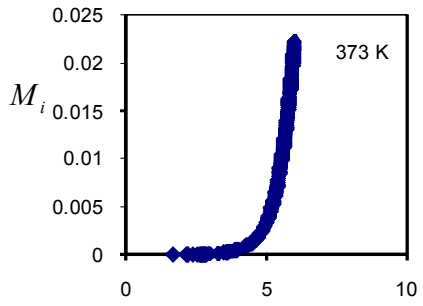

Figure 5.34 (*g*)

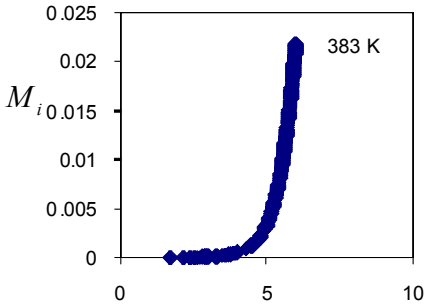

Figure 5.34 (*h*)

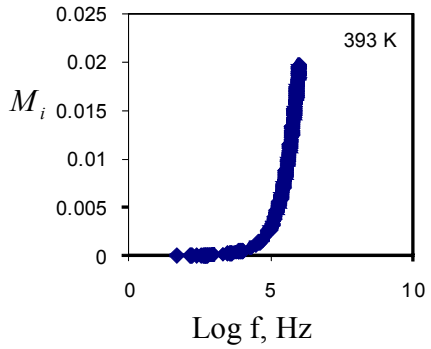

Figure 5.34 (*i*)

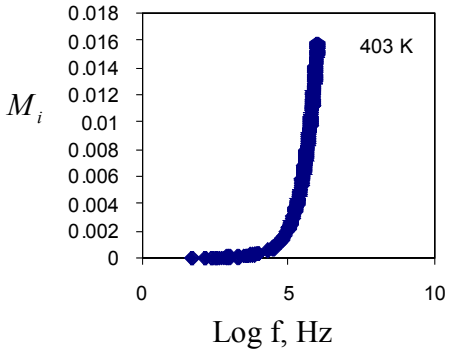

Figure 5.34 (*j*)

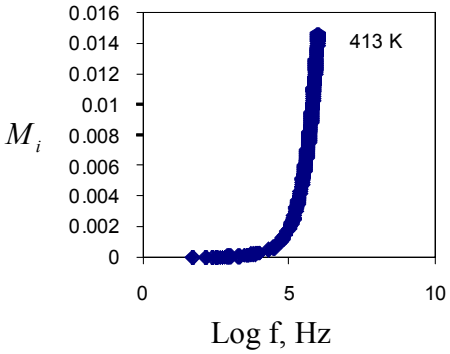

Figure 5.34 (*k*)

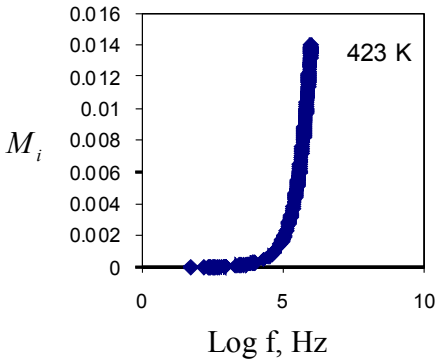

Figure 5.34 (*l*)

Figure 5.34: Plots of imaginary part of modulus with frequency at several temperatures for 0.4CuI-0.6AgI.

There is no peak observed for 0.3CuI-0.7AgI and 0.4CuI-0.6AgI. These samples amy have become mixed conductors.

From the figures shown above, M_r and M_i do show an increment at high frequency end. One can conclude that the AgI-CuI mixtures are ionic conductors as the modulus formalism shows the possible presence of peaks at higher frequencies for all AgI-CuI mixtures and temperatures. When temperature increases, the height of the peak decreases with addition of CuI into AgI.

In order to compare the modulus curves, the data points were superimposed by rescaling the axes. The scaling was done by dividing the $M_i(\omega)$ with $M_{i(\max)}(\omega)$. The frequency dependence of normalized imaginary part of $\frac{M_i(\omega)}{M_{i(\max)}(\omega)}$ for the highest conducting sample in the binary system at different temperatures is shown in figure below. The modulus curve shifts to a higher frequency as the temperature increased. This implies that the conductivity of the charge carrier is thermally assisted.

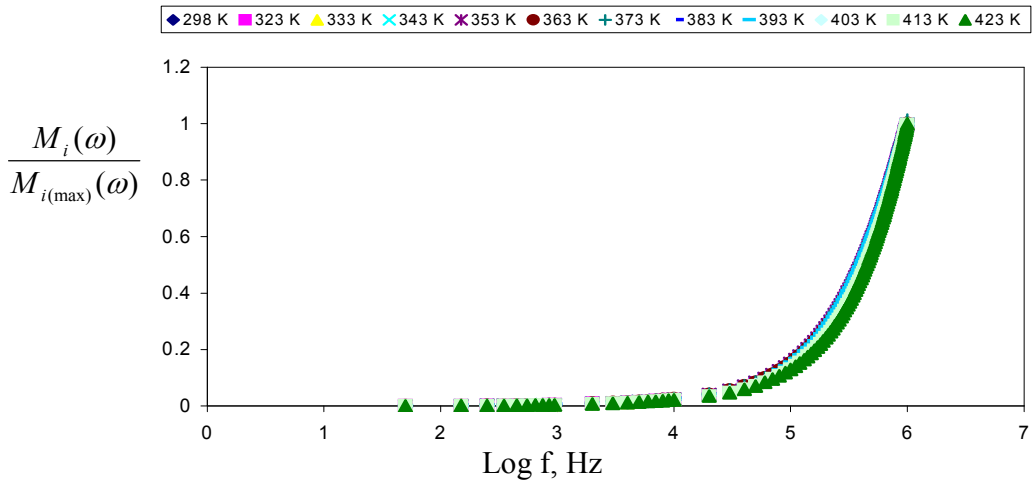

Figure 5.35: Normalized modulus M_i spectra for highest conducting sample in the AgI-CuI mixture at different temperatures.

5.6 Summary

The frequency dependence of dielectric constant, ε_i and dielectric loss, ε_r of AgI-CuI binary system at different weight percentages shows that the dielectric constant and dielectric loss increase as the frequency decreases. From $\ln \varepsilon_i$ versus $\ln \omega$ graphs, the frequency exponent, s was obtained. It is inferred that the ion transport in the AgI-CuI system occurs following the QMT model.

The plot of normalized electric modulus at different temperatures for the highest conducting sample for the binary system shows near perfect overlaps of the superimposed curves indicating that all the dynamic processes occurring at different frequencies exhibit the same thermal activation energy.